

RESEARCH ARTICLE

10.1002/2016JD025967

South Asian summer monsoon breaks: Process-based diagnostics in HIRHAM5

Key Points:

- Excess rainfall over tropical ocean regions contributes to climatological dry bias over central India in HIRHAM5
- MSE budget shows that anomalous dry advection (radiative cooling) is the leading process in initiating (maintaining) breaks
- Inconsistent relationship between anomalous rainfall and radiative cooling during breaks suggests weak moisture-radiation interaction

Correspondence to:

F. S. Hanf,
fhanf@hawaii.edu

Citation:




Hanf, F. S., H. Annamalai, A. Rinke, and K. Dethloff (2017), South Asian summer monsoon breaks: Process-based diagnostics in HIRHAM5, *J. Geophys. Res. Atmos.*, 122, 4880–4902, doi:10.1002/2016JD025967.

Received 20 SEP 2016

Accepted 20 APR 2017

Accepted article online 25 APR 2017

Published online 12 MAY 2017

Franziska S. Hanf^{1,2} , H. Annamalai^{1,3}, Annette Rinke² , and Klaus Dethloff² 

¹International Pacific Research Center, University of Hawaii at Mānoa, Honolulu, Hawaii, USA, ²Alfred Wegener Institute, Helmholtz Centre for Polar and Marine Research, Potsdam, Germany, ³Department of Oceanography, University of Hawaii at Mānoa, Honolulu, Hawaii, USA

Abstract This study assesses the ability of a high-resolution downscaling simulation with the regional climate model (RCM) HIRHAM5 in capturing the monsoon basic state and boreal summer intraseasonal variability (BSISV) over South Asia with focus on moist and radiative processes during 1979–2012. A process-based vertically integrated moist static energy (MSE) budget is performed to understand the model's fidelity in representing leading processes that govern the monsoon breaks over continental India. In the climatology (June–September) HIRHAM5 simulates a dry bias over central India in association with descent throughout the free troposphere. Sources of dry bias are interpreted as (i) near-equatorial Rossby wave response forced by excess rainfall over the southern Bay of Bengal promotes anomalous descent to its northwest and (ii) excessive rainfall over near-equatorial Arabian Sea and Bay of Bengal anchor a “local Hadley-type” circulation with descent anomalies over continental India. Compared with observations HIRHAM5 captures the leading processes that account for breaks, although with generally reduced amplitudes over central India. In the model too, anomalous dry advection and net radiative cooling are responsible for the initiation and maintenance of breaks, respectively. However, weaker contributions of all adiabatic MSE budget terms, and an inconsistent relationship between negative rainfall anomalies and radiative cooling reveals shortcomings in HIRHAM5's moisture-radiation interaction. Our study directly implies that process-based budget diagnostics are necessary, apart from just checking the northward propagation feature to examine RCM's fidelity to simulate BSISV.

1. Introduction

1.1. Background

Given that the seasonal monsoon rainfall during June–September (JJAS), which accounts for about 70–80% of the total annual rainfall over a major part of continental India dictates the agriculture and socioeconomic sectors of the country, model simulations of the South Asian summer monsoon (SASM) intraseasonal variability at very high spatial resolution are of crucial importance. Within the monsoon season, the rainfall fluctuates between periods of enhanced rainfall (active phases) and reduced rainfall (break phases) [Ramamurthy, 1969]. While the active/break cycle is characteristic of the nature of monsoons, long periods of sparse rainfall or extended breaks (lasting seven or more days) often result in severe droughts and famines [Raghavan, 1973; Prasanna and Annamalai, 2012]. Due to the occurrence of monsoon active/break phases on intraseasonal time scales bridging weather and climate, an accurate simulation of their characteristics would have an immense value on the ability to forecast monsoon rainfall over India. In climate models, however, realistic simulation of space-time evolution of monsoon intraseasonal variability is still in its infancy [e.g., Sperber *et al.*, 2013]. Here a high-resolution regional downscaling approach is attempted to assess the model's ability in capturing regional features associated with monsoon breaks, and process-based diagnostics are then applied to understand representations of moist and radiative processes in the model.

Past studies have recognized that the equatorial eastward propagating Madden-Julian oscillation (MJO) interacts with the monsoon by displaying northward propagation over South Asian longitudes and north-northwest migration over the tropical west Pacific [Yasunari, 1979; Sikka and Gadgil, 1980; Annamalai and Slingo, 2001]. In recent times, a leading idea to explain the existence and properties of the MJO describes the oscillation as a moisture mode. Briefly, MJO is considered as a disturbance regulated by processes controlling the tropospheric humidity under the weak temperature gradient approximation, and its existence requires charging and discharging of column-integrated moist static energy (MSE) [e.g., Raymond *et al.*, 2009;

Maloney, 2009; Sobel and Maloney, 2012]. In this framework, such disturbances can be destabilized by thermodynamic feedbacks, namely, surface turbulent fluxes and radiative cooling (sources and sinks of MSE) that result in the growth of MSE anomalies [e.g., *Hannah and Maloney, 2011*]. Diagnosing column-integrated MSE budgets on model simulations or reanalysis products, horizontal moisture advection has been found to explain the propagation of MJO [e.g., *Maloney, 2009; Andersen and Kuang, 2012; Kiranmayi and Maloney, 2011*].

Invoking similar ideas and considering the northward propagating convective anomalies as moisture modes, *Boos and Kuang [2010]* emphasized the role of moisture-radiation feedback in the destabilization process using a cloud system-resolving model. In a suite of climate model simulations, *Ajayamohan et al. [2011]* identified the advection of anomalous moisture by climatological winds as a mechanism for promoting the northward migration. By performing moisture and MSE budgets on reanalysis and climate model simulations, *Prasanna and Annamalai [2012]* showed that dry advection is the principal moist process in initiating while radiative cooling is the dominant MSE term in the maintenance of extended monsoon breaks over central India.

Undoubtedly, the three-dimensional moisture and zonal vertical easterly shear distributions in the time-mean over the monsoon region exert considerable effect on the life cycle of boreal summer intraseasonal variability (BSISV) [*Wang and Xie, 1997; Sperber and Annamalai, 2008*]. In this context, it is fair to mention that in climate models, limitations in BSISV simulations can be attributed to models' fidelity in realistically simulating the heterogeneous precipitation distribution over the broader Asian monsoon region. Despite considerable efforts, model systematic errors in the simulation of monsoon precipitation climatology still persist [e.g., *Sperber et al., 2013*]. Even though compared to Coupled Model Intercomparison Project 3 (CMIP3) the models in CMIP5 have shown improved skill at, for example, representing the northward propagation of convection, there is no single model that best represents all of the monsoon features [*Sperber et al., 2013*].

Does higher horizontal resolution improve monsoon precipitation simulation? South Asia is characterized by a complex orography and extensive mountain ranges of the Hindu Kush-Himalayas. *Boos and Hurley [2013]* emphasized the importance of a realistic representation of topography to reduce the common dry bias over continental India found in many CMIP models. While global climate models (GCMs) fail to adequately capture the orographic-induced rainfall arising partly due to the coarse resolution [*Sperber and Annamalai, 2008; Lucas-Picher et al., 2011*], there is a suggestion that global climate simulations with higher horizontal resolution (~ 20 km [*Rajendran et al., 2012*] and ~ 35 km [*Sabin et al., 2013*]) do resolve them but at the expense of high computational power. Regional climate models (RCMs) provide an alternative approach by dynamically downscale a global climate model simulation or a reanalysis [*Rummukainen, 2010*], an approach adopted here.

Several studies showed that RCMs have been fairly successful in representing spatial distribution of monsoon precipitation climatology over South Asia compared to that simulated by GCMs [e.g., *Dobler and Ahrens, 2010; Lucas-Picher et al., 2011; Dash et al., 2012; Befort et al., 2016*]. But, there are relatively few RCM attempts to address intraseasonal variability. *Dash et al. [2012]* analyzed the number of monsoon active and break phases and found that the modeled active phases are of shorter life span than those actually observed. On the other hand, *Befort et al. [2016]* diagnosed fidelity of their RCM in simulating the northward propagation of BSISV and found a well represented coupling between atmospheric circulation anomalies and rainfall anomalies over India on the intraseasonal timescale, especially during break events. However, no RCM study exists, which focuses on the identification of the processes that initiate and maintain monsoon breaks, and thereby addresses the strengths and weaknesses in the RCM physics. In doing so, we employ an atmospheric RCM, HIRHAM5 (discussed in section 2) that has been successfully applied to examine atmospheric and land surface characteristics over the Arctic region [*Zhou et al., 2014; Sommerfeld et al., 2015; Klaus et al., 2016*]. Using a previous version of the RCM at around 50 km horizontal resolution driven by ERA-40 reanalysis over the South Asian monsoon region, *Polanski et al. [2010]* demonstrated that the model is able to reproduce the topographic precipitation features and also noticed too wet conditions over the southern Arabian Sea and the Bay of Bengal windward of high mountains.

1.2. Present Study

Here we revisit the problem of high-resolution simulation of mean and intraseasonal variability of SASM precipitation and apply vertically integrated MSE budget (equation (2) in section 2), a process-based diagnostic that assess the representation of both physical parameterizations (diabatic sources) and dynamical core (adiabatic terms) employed in our RCM. First, we carry out a HIRHAM5 simulation with a horizontal resolution of 0.25° (~ 25 km), driven by ERA-Interim products (~ 25 km, interpolated from ~ 80 km resolution) for

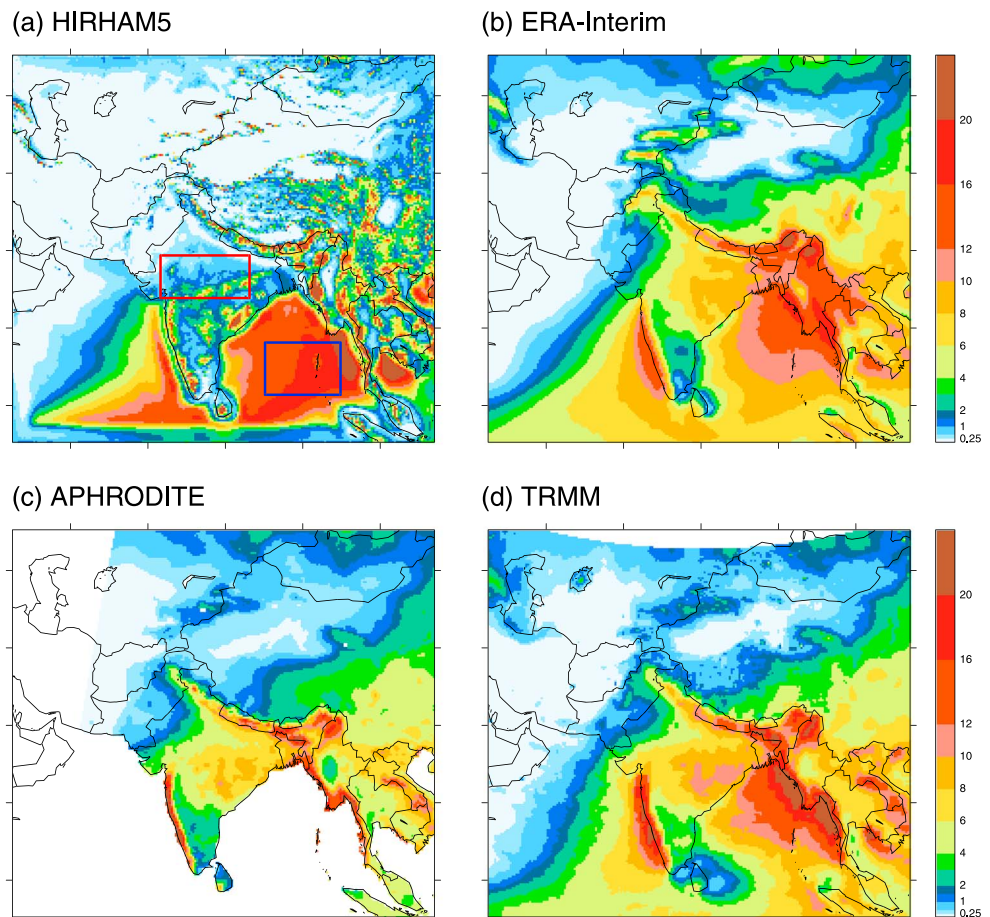


Figure 1. June–September averaged precipitation climatology (mm d^{-1}), from (a) HIRHAM5 (1979–2012) and (b) ERA-Interim (1979–2012) and from the observational products (c) APHRODITE (1979–2007) and (d) TRMM (1999–2012). The red and dark blue boxes indicate the central India (21° – 27°N , 72° – 85°E) and Bay of Bengal (7° – 15°N , 87° – 101°E) regions, respectively.

the period 1979–2012. Is the RCM resolution (~ 25 km) adequate enough to resolve regional rainfall features of the mean monsoon? As a prerequisite for a successful simulation of BSISV [Sperber and Annamalai, 2008], we assess the model's ability in capturing a realistic time-mean basic state by examining the observed precipitation distribution (Figure 1d) including that of orographically induced heavy precipitation surrounding continental India, and the regional west (dry)–east (moist) gradient in the simulated monsoon precipitation climatology. Further, we interpret model's capability in terms of vertical distribution of climatological moisture, temperature, vertical pressure velocity, and conditionally averaged precipitation in bins of column water vapor (CWV). Our results reveal a dry bias over central India, while excessive rainfall exists over the southern Bay of Bengal and the near-equatorial Arabian Sea. We propose the hypothesis that the drying over central India is likely caused by a Rossby wave response [Gill, 1980; Rodwell and Hoskins, 1996] to the surplus of rainfall and associated diabating heating over the southern Bay of Bengal. To test this, we perform sensitivity experiments with a linear baroclinic atmosphere model (LBM).

Second, encouraged by studies that explored the processes that account for monsoon breaks over central India, we identify model captured break events and construct composite evolution of key variables and then apply MSE budget to the modeled breaks in order to isolate and quantify the relative contributions of diabatic and adiabatic terms in anchoring MSE anomalies. ERA-Interim has been widely used to diagnose MSE budget during both summer and winter intraseasonal variability [e.g., Maloney, 2009; Prasanna and Annamalai, 2012]. Being aware that HIRHAM5 is driven by a reliable performing model, we expect that the applied diagnostics will help to identify model limitations and provide pathways for model improvement. In deep tropics, surface precipitation is directly proportional to vertical advection of MSE. Also note that MSE terms such as surface

fluxes and radiative fluxes (equation 2, diabatic terms) reflect leading physical parameterizations employed in climate models. Our results show that HIRHAM5 is able to capture the leading processes accountable for the initiation (anomalous dry advection) and maintenance (net radiative cooling) of monsoon breaks over central India. However, reduced contributions of all adiabatic terms in the MSE budget and an inconsistent relationship between the anomalous precipitation term and the net radiative flux term during the break cycle suggest weakly represented moisture-radiation interactions in HIRHAM5.

Section 2 outlines the RCM, the simulation setup, and the data used and presents a brief description of the diagnostic methods applied. Section 3 provides an overview of the model's fidelity in simulating the basic state of the SASM. Evaluation of the monsoon break pattern captured by the model is shown in section 4, followed by the results of the MSE budget in section 5. The study completes with a short summary and a discussion in section 6.

2. Model, Data, and Method

In this section, a brief discussion on the configuration, numerics and physical parameterizations employed in HIRHAM5 is provided (section 2.1) followed by a description of the reanalysis and observational data sets used to validate the model simulations (sections 2.2). Then, a short overview of the LBM and the design of hypothesis-testing experiments is given (section 2.3). Finally, the method employed to identify monsoon breaks and the MSE budget study to reveal the leading processes responsible for the rainfall anomalies over central India during breaks are presented (section 2.4).

2.1. Regional Climate Model and Simulation Setup

For this study, the version 5 of the atmospheric RCM HIRHAM (HIRHAM5) [Christensen *et al.*, 2007], which combines the dynamical core of the regional weather forecast model HIRLAM7 (High Resolution Limited Area Model version 7) [Undén *et al.*, 2002] and the physical parameterization package of the atmospheric general circulation model European Centre/Hamburg model version 5 (ECHAM5) [Roeckner *et al.*, 2003] is applied.

HIRHAM5's integration domain covers the whole South Asia including the Himalayas (between $\sim 0^\circ\text{N}$ and 48°N and 42°E to 119°E ; Figure 1a) with 218×200 grid cells arranged in a rotated coordinate system. The model simulation was performed at a horizontal resolution of 0.25° (~ 25 km) in rotated longitude and latitude, and 40 nonequidistant levels given in sigma-pressure hybrid coordinates with the top level at 10 hPa. The model output is saved daily for single levels (including surface variables), 40 vertical model levels, and 15 vertical pressure levels: 70, 200, 250, 300, 500, 600, 700, 800, 850, 875, 900, 925, 950, 975, and 1000 hPa. Here the choice of the model domain is motivated by the set up of an earlier study [Polanski *et al.*, 2010] with the previous version of the model.

The hydrostatic model HIRHAM5 solves seven prognostic equations for the horizontal wind components, temperature, specific humidity, cloud liquid water content, cloud ice content, and surface pressure. An implicit sixth-order horizontal diffusion scheme is applied to each prognostic model variables except surface pressure, to prevent the accumulation of energy of the smallest scales. In order to maintain model stability, we use a model configuration with a diffusion coefficient of $K_g = 1.0 \times 10^{27}$, while $K_g = 1.0 \times 10^{24}$ is the default configuration of HIRHAM5. For the horizontal discretization of the equations a centered finite difference scheme is implemented. Following the approach by Sass *et al.* [2002], an upstream advection scheme is used for the cloud liquid water content and cloud ice content in order to improve advection characteristics. Both schemes are applied on an Arakawa C grid. The temporal discretization is performed with a semi-implicit leapfrog scheme at an integration time step of 120 s. To be consistent with the horizontal discretization, the calculation of the tendencies of cloud liquid water content and cloud ice content is treated differently by using an explicit Euler forward method without any semi-implicit correction. The HIRHAM5 simulation has been carried out for the time period of 1979–2012.

Cumulus convection is represented in HIRHAM5 by a modified version of the Tiedtke mass flux scheme [Tiedtke, 1989; Nordeng, 1994], which distinguishes between shallow, midlevel, and deep convection. The scheme describes cumulus clouds by a bulk model including the effects of entrainment and detrainment processes on the updraft and downdraft mass fluxes. Convective activity of deep convection is related to the degree of convective instability and hence limited by a characteristic time at which the convective available potential energy (CAPE) can be consumed. The parameterization of stratiform clouds consists of three components: prognostic equations for the water phases (vapor, liquid, and solid), the bulk cloud

microphysics scheme of *Lohmann and Roeckner* [1996], and the prognostic-statistical cloud cover scheme of *Tompkins* [2002]. The microphysics scheme takes into account phase changes between the water states (condensation/evaporation, deposition/sublimation, and freezing/melting) and precipitation formation processes (autoconversion, aggregation, and accretion) as well as further processes like evaporation of rain, melting of snow, and sedimentation of cloud ice. HIRHAM5 includes a six-band shortwave radiation model of *Fouquart and Bonnel* [1980], and a longwave radiative transfer parameterization following the rapid radiative transfer model developed by *Mlawer et al.* [1997]. Aerosol distributions are prescribed using the Tanré climatology [*Tanré et al.*, 1984], which provides aerosol radiative properties for mixtures of maritime, continental, urban, desert, and background aerosols, but neglects seasonal variations. The land surface temperature is calculated from the surface energy balance, linking the atmosphere and the underlying land surface by using an implicit scheme [*Schulz et al.*, 2001] which allows synchronous calculation of the prognostic variables and the surface fluxes. Soil temperatures are modeled over five unevenly spaced layers using a thermal diffusion equation, and the soil hydrology is parameterized by a simple single-layer bucket model that takes into account four water reservoirs: liquid water at the canopy, snow at the canopy, snow at the surface, and soil water. Most of the land surface parameters (e.g., vegetation ratio, leaf area index, forest ratio, and background albedo) are prescribed from a global 1 km resolution data set compiled by *Hagemann* [2002]. Physical parameterizations do not include the momentum transports due to subgrid-scale gravity waves.

Initialization and 6-hourly prescribed lateral boundary forcing data are obtained from the ERA-Interim [*Dee et al.*, 2011], the latest global atmospheric reanalysis produced by the European Centre for Medium-Range Weather Forecasts (ECMWF). In order to prevent numerical instabilities between the driving field and the regional model [*Rummukainen*, 2010], the information from the lateral boundaries is transferred to the inner model domain by a boundary relaxation method developed by *Davies* [1976] using a buffer zone size of 10 grid cells. Further, a 1% nudging is applied using the dynamical relaxation technique [*Davies and Turner*, 1977] at all levels in the inner model domain. At the lower boundary the model is driven by 6-hourly interpolated sea surface temperatures (SSTs) based on daily ERA-Interim reanalysis.

2.2. Validation Data

To evaluate the performance of HIRHAM5, different reference data sets (reanalysis, gauges-based, and satellite data) are taken into account. The bulk of atmospheric data used for the validation comes from the ERA-Interim reanalysis. Reanalyses can provide a temporally coherent and spatially complete record but over the data-sparse monsoon region, records are influenced by model prejudices of the data assimilation system [e.g., *Annamalai et al.*, 1999] resulting in MSE budget residuals [*Prasanna and Annamalai*, 2012]. To ensure consistency with the model's spatial resolution, the ERA-Interim products were interpolated at the ECMWF onto a $0.25^\circ \times 0.25^\circ$ grid with 40 vertical levels during 1979–2012.

For precipitation and to conform with model resolution, two additional data sets at $0.25^\circ \times 0.25^\circ$ are used: (i) gridded daily precipitation based on rain gauge observations from the Asian Precipitation—Highly-Resolved Observational Data Integration Towards Evaluation (APHRODITE) of water resources project version V1101 for monsoon Asia [*Yatagai et al.*, 2012] for the period 1979–2007; and (ii) 3-hourly merged satellite precipitation product from the Tropical Rainfall Measuring Mission (TRMM) combined “TRMM and Other Satellite Precipitation Product” (3B42) [*Huffman et al.*, 2007] during 1998–2012.

2.3. Linear Baroclinic Model

The global LBM [*Watanabe and Jin*, 2003] is used for the hypothesis-testing sensitivity experiments. *Annamalai and Sperber* [2005] employed the LBM as a diagnostic tool to understand the mutual interactions among the regional rainfall anomalies at intraseasonal timescales. In order to see if the excess rainfall and associated diabating heating over the southern Bay of Bengal force a Rossby wave pattern with descent over central India, two LBM experiments were carried out. In both experiments, the magnitude and shape of HIRHAM5's climatological positive precipitation bias (HIRHAM5 minus ERA-Interim) was used to force the LBM selectively in two regions: (a) only over the Bay of Bengal and (b) over the whole HIRHAM5's model domain. The vertical heating profile of the forcing function has a maximum at 400 hPa. The forcing was kept throughout the model integration (29 days), and the LBM's steady state responses averaged for days 24–29 are used for detailed analysis. Since HIRHAM5 is driven at lateral boundaries by ERA-Interim (section 2.1), LBM is linearized with ERA-Interim climatology. The horizontal resolution of LBM used here is T42, and the model is configured with 20 levels in the vertical.

2.4. Diagnostic Methods

2.4.1. Identification of Breaks

Monsoon breaks are identified following *Prasanna and Annamalai* [2012]. By using daily total precipitation from HIRHAM5, a monsoon break event is defined, if for at least three consecutive days precipitation anomalies averaged over central India (21° – 27° N, 72° – 85° E; Figure 1a) are below one standard deviation. Hence, only break events that persist for three or more days are identified, and composites of breaks are constructed based on all identified break events (27 break events). The inspection of monsoon breaks focuses on the period 1 July to 17 September, the established phase of the monsoon over central India in HIRHAM5, to avoid the selection of break events during the local onset and withdrawal phases. In order to identify precursors and to present the life cycle of monsoon breaks, lag composites are generated from -20 days to $+15$ days with “day 0” corresponding to the peak of the break phase, i.e., the day with the maximum amplitude of precipitation anomalies over central India. To circumvent possible noise that can modulate regional features, a 5 day running mean is applied on the results shown and discussed here.

2.4.2. Budget Diagnostics

To identify processes that contribute to precipitation anomalies, we perform MSE budget diagnostics that combines physical processes influencing moisture and temperature [*Su and Neelin*, 2002]. The interaction between cumulus convection and large-scale circulation is fundamental in the tropics, and such a representation requires consideration of moisture and temperature [*Back and Bretherton*, 2006]. Both become linked in the quantity of the MSE. *Annamalai* [2010] applied MSE budget to examine moist processes that account for monsoon interannual variability, while *Prasanna and Annamalai* [2012] invoked the budget analysis to understand processes during extended monsoon breaks.

The MSE, m , is given by

$$m = s + Lq \quad (1)$$

with $s = c_p T + gz$ is the dry static energy (DSE), where c_p is the specific heat capacity at constant pressure, T is the temperature, g is the acceleration due to gravity, and z is the geopotential height. Also, L is the latent heat of condensation, and q is the specific humidity. Vertically integrated, the anomalous MSE tendency (or storage term) is approximately given by

$$\left\langle \frac{\partial m}{\partial t} \right\rangle' = -\left\langle \omega \frac{\partial m}{\partial p} \right\rangle' - \left\langle \mathbf{v} \cdot \nabla m \right\rangle' + LW' + SW' + H' + E' \quad (2)$$

where ω' is the anomalous vertical pressure velocity, \mathbf{v}' is the anomalous horizontal velocity vector, and ∇ is the gradient operator. Note that equation (2) includes both adiabatic terms (first and second term on the right-hand side) and diabatic terms (third to sixth term on the right-hand side). LW' and SW' are the anomalous net radiative longwave and shortwave heating rates, and their sum accounts for the anomalous net radiative flux into the atmospheric column F'_{rad} . Also, H' and E' represent the anomalous surface sensible and latent heat fluxes, respectively. The symbols $\langle \rangle'$ denote vertical integration from 1000 hPa to 10 hPa. Quantities with a prime mark represent daily anomalies for break days calculated as a difference between the daily values and the daily climatology (daily value minus corresponding daily climatology). The term $-\left\langle \omega \frac{\partial m}{\partial p} \right\rangle'$ defines MSE divergence or its vertical advection and is proportional to precipitation anomalies, while the horizontal advection of MSE $-\left\langle \mathbf{v} \cdot \nabla m \right\rangle'$ can be split into horizontal advection of temperature $-\left\langle \mathbf{v} \cdot \nabla T \right\rangle'$ and moisture $-\left\langle \mathbf{v} \cdot \nabla q \right\rangle'$. Equation (2) links the temperature budget and the moisture budget, thereby seeking thermodynamic balance required in tropical phenomena. Here the MSE budget diagnostics are estimated with daily data, and then 5 day running means are constructed and presented for discussions. The temporal evolution of the storage term as well as the budget residuals are estimated, and their implications for the present research are discussed. Readers are referred to *Su and Neelin* [2002] and *Maloney* [2009] for details on the budget procedures.

3. HIRHAM5 Basic State Results

Figure 1 shows the mean JJAS climatology of precipitation from HIRHAM5 (a), ERA-Interim (b), APHRDITE (c), and TRMM (d). Both in spatial structures and magnitude, there is good agreement between the two observations (Figures 1c and 1d), while the structure in ERA-Interim (Figure 1b) agrees with observations, the intensity of precipitation does not (e.g., dry bias over central India, wet bias over plains of Indo-China, southern Bay

of Bengal, and southeastern Arabian Sea). The HIRHAM5 precipitation climatology (Figure 1a) captures the observed orographically induced rainfall belts at the foothills of the Himalayas, along the Western Ghats, and the Arakan Range and Tenasserim Range in Burma. However, as in ERA-Interim, HIRHAM5 produces excess (rather unusually high) rainfall over the open oceans of the southern Bay of Bengal and southeastern Arabian Sea. Similar biases are noted in high-resolution runs of the atmospheric general circulation model ECHAM5 [Hagemann *et al.*, 2006], and these biases are in close correspondence to overestimated shortwave cloud forcing [Wild and Roeckner, 2006]. Hagemann *et al.* [2006] supposed that the hydrological cycle is too strong in ECHAM5 due to insufficient atmospheric absorption by water vapor, aerosols, and clouds in the radiation physics. Note that the radiation physics package employed in HIRHAM5 is taken from that used in ECHAM5.

Another striking mismatch in HIRHAM5's bias pattern is the rather noisy precipitation (Figures 1a and 13) in regions of steep slopes (also found in ω , Figure 2c). Gollvik [1999] found similar small-scale noise pattern in high-resolution rainfall forecasting experiments of the numerical weather prediction model HIRLAM over the Scandinavian mountain region using three different horizontal resolutions (22 km, 11 km, 5.5 km) and suggested the sensitivity of the convection parameterization as one reason for the lack of improvements of higher resolutions. Further, he assumed that a part of this noise is created by an orographic forcing that cannot be handled by the model dynamics. Note that HIRHAM5 uses the dynamics of HIRLAM7. While fixing this model bias is important, it is primarily noted poleward of 28°N and therefore expected not to influence results over central India.

Figure 2 compares the mean JJAS basic state of the SASM from HIRHAM5 (a–c) with that from ERA-Interim (d–f) for selected atmospheric variables. Similarly, Figure 3 compares vertical profiles of key MSE variables averaged over central India and Bay of Bengal (7°–15°N, 87°–101°E; Figure 1a). HIRHAM5 captures salient features of the monsoon, including the surface heat low over northwestern India and Pakistan (not shown), the low-level westerly jet over the northern Arabian Sea (Figures 2a and 2d), an important element in feeding moisture to the monsoon convection, as well as the Tibetan anticyclone and easterly jet at high levels (not shown). The model biases in precipitation over the open oceans (Figure 1a) are readily accounted for by excessive CWV (Figure 2b) and enhanced vertical pressure velocity (ω) at midtropospheric level (Figure 2c). The vertical profile of ω averaged over Bay of Bengal (Figure 3b) clearly indicates a “top-heavy” structure, illustrating elevated latent heating due to combined effects of deep convection and stratiform precipitation. In sharp contrast to that, over central India (Figure 3a), both model and ERA-Interim vertical profiles of ω depict a “bottom-heavy” structure with a maximum around 850 hPa/875 hPa for ERA-Interim/HIRHAM5 with the model values indicating a rapid transition to near-zero and climatological descent upward of ~600 hPa. Over continental India, the model simulated reduced CWV (Figure 2b) is consistent with reduced moisture content in the boundary layer (Figure 3c). Compared to reanalysis, warm (Figure 3d) and dry (Figure 3c) lower tropospheric layers would impact the model simulated convective instability and CAPE, factors that will limit the vertical growth of clouds. Subsequently impacting latent heat release and vertical profile of ω .

3.1. Proposed Hypotheses

The results presented so far reveal a climatological dry bias over central India, while a wet bias is simulated over the southern Bay of Bengal and the near-equatorial Arabian Sea during the summer monsoon season in HIRHAM5. Could be the excess rainfall over the open oceans the cause for the anomalous drying? Annamalai [2010] showed that the Asian summer monsoon is determined by three regional heat sources, the western tropical Pacific, the central India region extending into the head of Bay of Bengal, and the equatorial Indian Ocean, and showed in doing LBM experiments that any forcing which modifies one of these heat sources (intensity or spatial distribution) can influence the monsoon rainfall pattern through the interaction between equatorial waves and moist physics. The excessive precipitation bias over the Bay of Bengal centered around 6°–8°N in HIRHAM5 (Figures 1a and 13a), based on linear theory and in a resting atmosphere [Gill, 1980], is expected to force a Rossby wave response to the northwest of the heating maximum. This response is intensified in the northern hemisphere if the summer mean (June–September) flow is prescribed in the linear model [Rodwell and Hoskins, 1996]. Invoking these ideas, we hypothesize that excessive precipitation over the Bay of Bengal in HIRHAM5 would force a Rossby wave pattern with descent over central India. Further, we hypothesize that the surplus of rainfall over the southern Bay of Bengal and the near-equatorial Arabian Sea would promote a local Hadley-type circulation bias in HIRHAM5 that may affect the mean monsoon ascent region over central India and hence the local rainfall pattern.

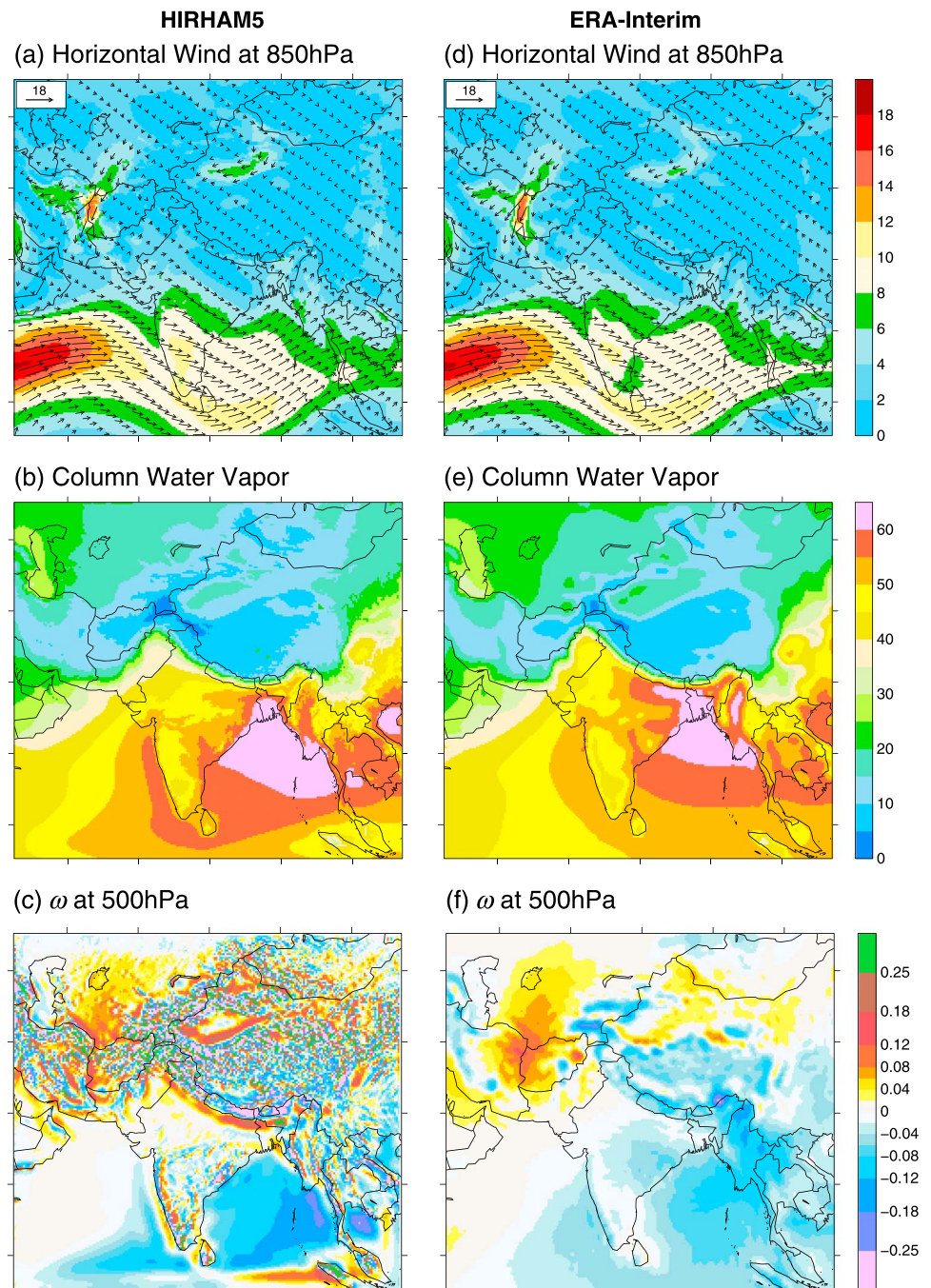


Figure 2. June–September averaged climatology, from (a–c) HIRHAM5 and (d–f) ERA-Interim, showing horizontal wind and horizontal wind speed (shading) at 850 hPa (m s^{-1}) (Figure 2a and 2d); column water vapor (kg m^{-2}) (Figure 2b and 2e), and vertical pressure velocity ω at 500 hPa (Pa s^{-1}) (Figure 2c and 2f). Scale vectors of Figures 2a and 2d 18 m s^{-1} are also shown.

In summary, we propose the following two hypothetical mechanisms: (i) excessive precipitation and associated diabatic heating over the southern Bay of Bengal force descent to its west, primarily over continental India (near-equatorial Rossby wave response); and (ii) excess precipitation over the near-equatorial Arabian Sea and Bay of Bengal anchors a local Hadley-type circulation with descent over continental India.

3.2. Validation of Hypotheses

To test the first hypothesis, the LBM is forced in two experiments with a diabatic heating anomaly proportional to HIRHAM5's mean monsoon positive precipitation bias in two different regions: the entire Bay of Bengal and

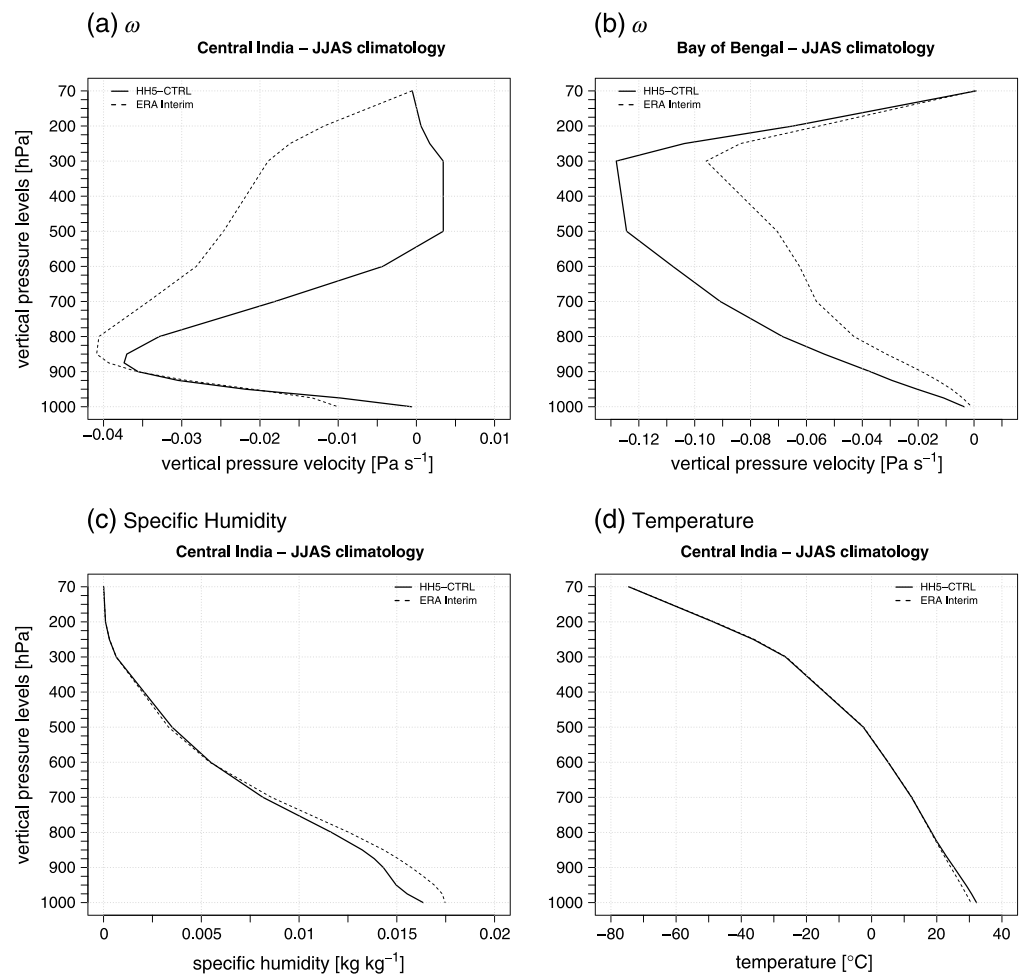


Figure 3. Vertical distribution of June-September averaged climatology for (a) vertical pressure velocity ω (Pa s^{-1}) averaged over central India (21° – 27°N , 72° – 85°E) and (b) averaged over Bay of Bengal (7° – 15°N , 87° – 101°E), (c) specific humidity (kg kg^{-1}) averaged over central India, and (d) temperature ($^{\circ}\text{C}$) averaged over central India from HIRHAM5 (solid line) and ERA-Interim (dashed line).

the whole HIRHAM5 model domain (including Arabian Sea and Bay of Bengal forcing). Since the steady state response between these two experiments (not shown) did not offer any notable differences, because of the dominance of the precipitation bias in HIRHAM5 over the Bay of Bengal, only the results of the Bay of Bengal forcing experiment is presented in Figure 4. Note that the LBM is linearized around the basic state (ERA-Interim here), and the steady state response obtained is “anomalous” [Watanabe and Jin, 2003]. In the LBM’s steady state solution of both the divergence (contour and shading in Figure 4a) and horizontal 850 hPa wind (arrows in Figure 4a) patterns suggest a direct response to the imposed heating. A low-level convergent flow and associated cyclonic vorticity is noticeable over the southeastern Bay of Bengal. In response to the applied forcing a divergent flow appears to the northwest encompassing central India with strongest signature over 19° – 24°N , 75° – 88°E , the region of maximum divergence at 850 hPa in Figure 4a. Figure 4b shows the anomalous LBM response of the vertical profile of omega averaged over this region (black dashed/dotted line) along with HIRHAM5’s bias (HIRHAM5 minus ERA-Interim) in the climatological vertical profile of omega averaged over central India (black solid line). While HIRHAM5’s omega bias reveals anomalous descent throughout the troposphere with a maximum around 500 hPa, the idealized solution from LBM depicts descent anomalies from about 750 to 70 hPa but with reduced amplitudes (with moderate ascent anomalies in the lower troposphere). Note that while HIRHAM5 is a regional climate model incorporating full physics and nonlinear interactions and feedbacks, the LBM lacks in such model configuration. Therefore, the magnitude of the LBM response is expected to be weaker compared to HIRHAM5. Barring smaller amplitudes, the results of the LBM

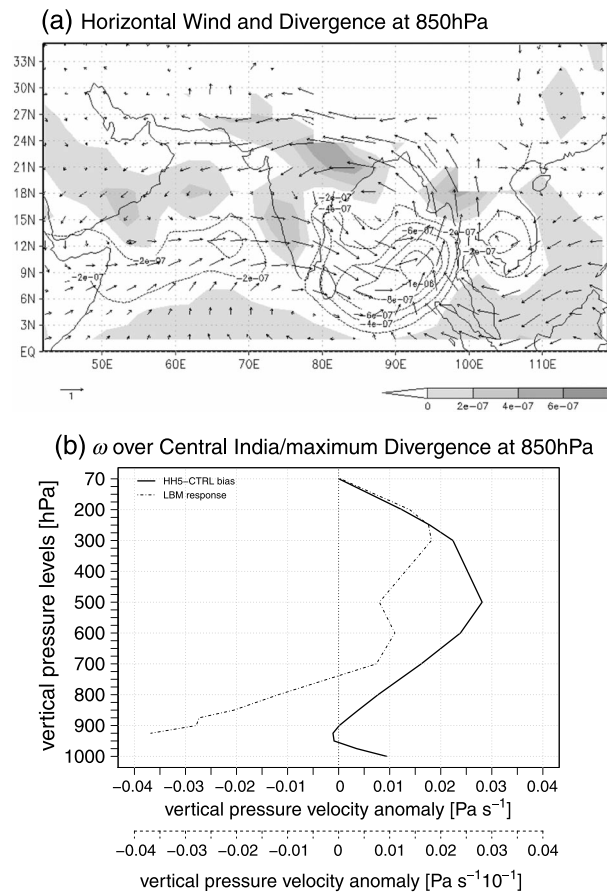


Figure 4. Anomalous LBM steady state response to an heating profile forcing with maximum at 400 hPa based on HIRHAM5’s JJAS climatological total precipitation bias over the Bay of Bengal averaged from 24 to 29 days (last 6 days) of LBM integration: (a) horizontal wind (m s^{-1}) and divergence (contour and shading) at 850 hPa and (b) vertical distribution of vertical pressure velocity ω ($\text{Pa s}^{-1} 10^{-1}$) averaged over maximum divergence at 850 hPa (19° – 24°N , 75° – 88°E ; Figure 4a) along with HIRHAM5’s JJAS climatological ω bias (HIRHAM5 minus ERA-Interim) (Pa s^{-1}) over central India. In Figure 4a, the positive values are shaded with an interval of $2\text{e}^{-7} \text{ s}^{-1}$ whereas the negative values are shown in contours with an interval of $-2\text{e}^{-7} \text{ s}^{-1}$. The scale vector of Figure 4a 1 m s^{-1} is also shown.

experiments do support our interpretation, i.e., HIRHAM5’s dry bias over central India is partly attributed to a Rossby wave descent forced by excess rainfall over the Bay of Bengal.

To support the second hypothesis, we averaged anomalous meridional and vertical velocity fields (difference between HIRHAM5 and ERA-Interim) over the Indian longitudes (68°E to 96°E) and show them in a vector form (as mass flux) and stream function form (Figure 5). There is a suggestion for an overturning circulation with anomalous ascent over the near-equatorial region (centered at around 6°N) and anomalous descent over central Indian latitudes (centered around 22°N), indicating a local Hadley-type circulation bias in HIRHAM5.

As a consequence, climatological descent occurs throughout the free troposphere leading to the dry bias in the simulated CWV, specific humidity, and finally rainfall over central and northwest India. Furthermore, we suggest that a part of the model’s bias pattern could cascade from the driving data (ERA-Interim), which show similar precipitation biases over the open oceans (Figure 1).

4. HIRHAM5 Break Pattern

To assess the model’s fidelity in simulating the space-time characteristics of breaks, Figure 6 shows composite spatial maps of precipitation (a–f) and 850 hPa horizontal wind (g–i) anomalies for HIRHAM5 from -20 days to $+5$ days. The maps corresponding to $+10$ days to $+20$ days are approximate mirror images and hence not shown. At -20 and -15 days, continental India experiences weak positive rainfall anomalies or an active phase of the monsoon (Figures 6a and 6b). During that time, negative rainfall anomalies are noticeable

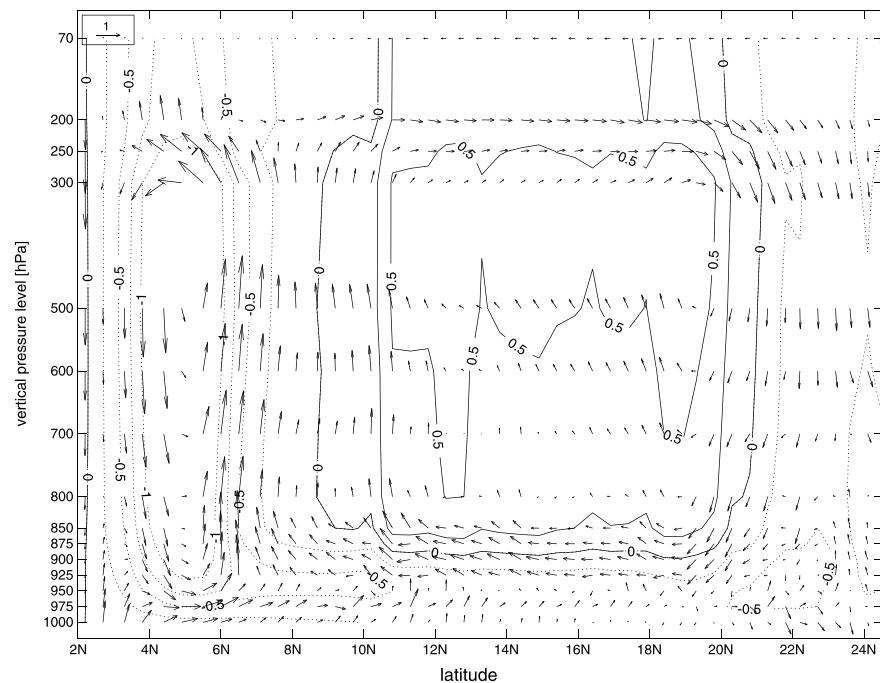


Figure 5. Mass flux in $\text{kg m}^{-2} \text{s}^{-1}$ (arrows) and stream function in $\text{m}^2 \text{s}^{-1}$ (contour) to illustrate a local Hadley-type circulation bias in HIRHAM5, where the anomalous vertical pressure velocity ω and meridional wind fields (difference between HIRHAM5 and ERA-Interim) are zonal averaged over the Indian longitudes (68° – 96°E). The ω component is scaled by a factor of 200 for the mass flux calculation to depict the overturning. The scale vector $1 \text{ kg m}^{-2} \text{ s}^{-1}$ is also shown.

over the eastern Arabian Sea aligned to the Western Ghats. Likely, in response to this stationary pattern of anomalous negative rainfall weak easterly low-level wind anomalies develop over the southern Arabian Sea (Figure 6h) suggesting a reduced moisture influx into the monsoon region by day -15 . From -15 days onward (Figures 6b–6e), negative rainfall anomalies spread northward leading to rainfall reduction over central India marking the transition from a monsoon active to a break phase. During their northward progression the negative precipitation anomalies grow in intensity and depict a spatial pattern with signatures along the Western Ghats, over central India, and over parts of the northern and eastern Bay of Bengal from day -5 to day $+5$ (Figures 6d–6f). To feature the poleward progression in HIRHAM5, Figure 7 shows a Hovmöller plot (latitude-time lag plot) of composite precipitation anomalies averaged over the Indian longitudes 70° – 90°E during model simulated monsoon breaks (from -20 days to $+20$ days). The model captures the steady poleward progression of negative precipitation anomalies with time indicated by the slope of the envelope of precipitation anomalies. However, unlike in observations [e.g., Krishnan *et al.*, 2000], precipitation anomalies in HIRHAM5 are not adequately reduced over the north and northwest of India (Figure 6e). In the model too, the intensified anomalous easterlies are part of a low-level anticyclonic circulation structure that develops as a Rossby wave response to suppressed convection over central India during the initiation phase of breaks at day -5 (Figure 6j). Further, at the same pentads, an anomalous cyclonic shear in association with positive rainfall anomalies can be found just north of the equatorial Indian Ocean. Suppressed precipitation over the Indian continent, while rainfall is enhanced over the oceanic regime, indicates the representation of the well-observed north-south dipole over the Indian latitudes [Sikka and Gadgil, 1980; Wang and Xie, 1997; Krishnan *et al.*, 2000; Annamalai and Slingo, 2001] in HIRHAM5. In summary, consistent with observations, the space-time evolution of composite precipitation anomalies constructed from HIRHAM5 reveals two major features: (i) there is a pronounced northward progression over India and the Bay of Bengal, representing the 40 day intraseasonal mode; and (ii) that the monsoon break phase over central India persists from at least -5 days to $+5$ days (Figures 6d–6f), which means for about 10 days. Encouraged by the overall success of the model simulated precipitation anomalies during breaks, next we discuss the temporal evolution of the anomalous stability conditions in the vertical that may well provide guidance to the initiation and maintenance of the breaks.

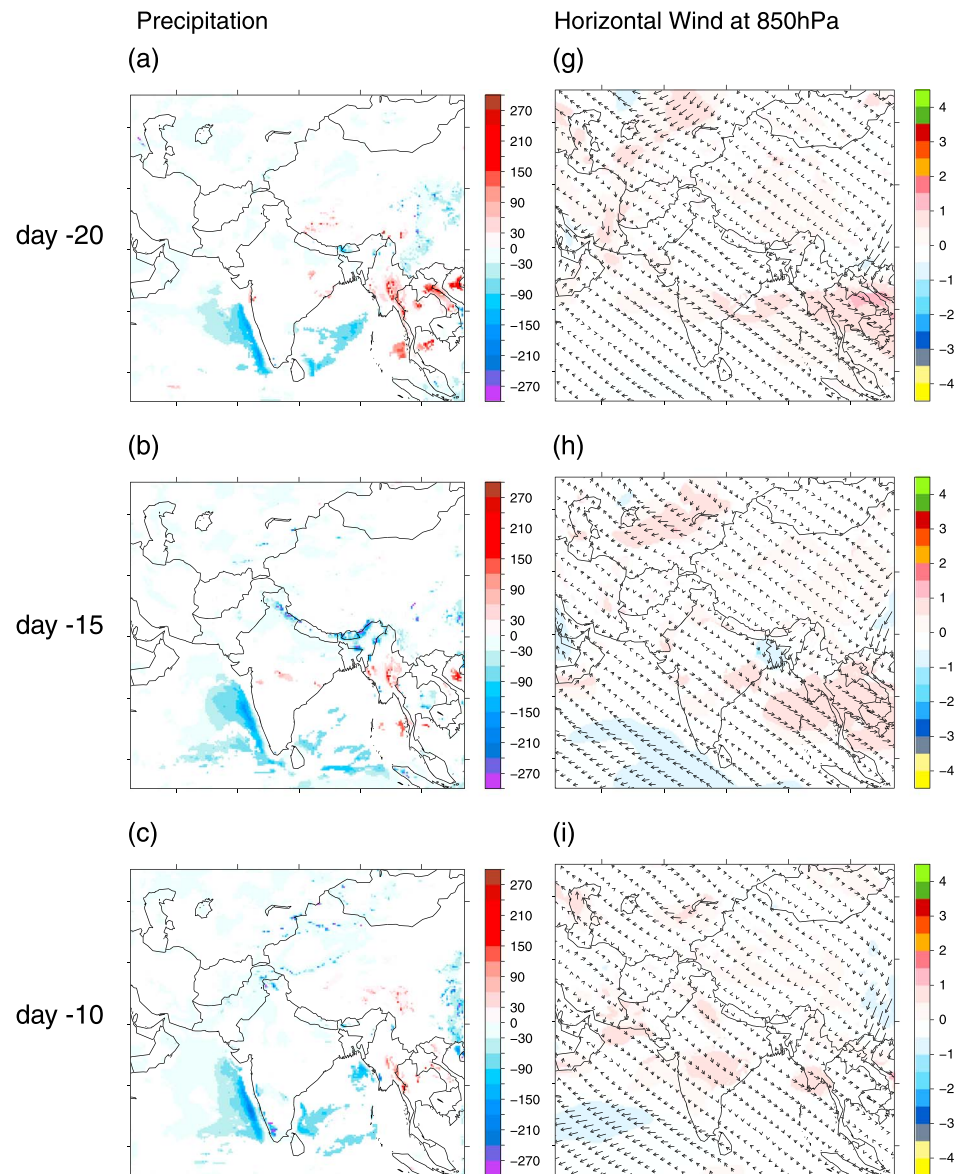


Figure 6. Space-time evolution of composite anomalies of (a–f) precipitation ($W m^{-2}$) and (g–i) horizontal wind and horizontal wind speed (shading) at 850 hPa ($m s^{-1}$) during breaks. Units of precipitation anomalies are in $W m^{-2}$ ($mm d^{-1} \times 28.93519$) so that around $29 W m^{-2}$ corresponds to around $1 mm d^{-1}$. The composites are shown from days -20 to days $+5$ with day 0 defined as the peak phase of monsoon breaks and maximum amplitude of rainfall anomalies. Each panel is 5 days apart. (k) A scale vector of $3 m s^{-1}$ is given. Only significant anomalies at a 95 % confidence level are shown and were calculated using a Student's t statistic.

Vertical profiles of ω , specific humidity, and temperature anomalies for HIRHAM5 from -15 days to day 0 (Figures 8a–8c) capture the progressive changes in the atmospheric stability over central India in association with breaks. The anomalous descent confined to 600–100 hPa at -15 days progressively extends to about 800 hPa at -10 days and then amplifies and stretches throughout the troposphere at -5 days (Figure 8a). At day 0, the anomalies further intensify and maximize around 800–700 hPa, just above the layers at which climatological ascent peaks (875–850 hPa; Figure 3a), but with weaker amplitudes compared with reanalysis (not shown).

The vertical patterns in anomalous specific humidity (Figure 8b) show drying through the entire column of the troposphere from 15 days to day 0. A possible interpretation is that during -15 days to -10 days, the weak upper troposphere drying is attributed to anomalous descent. At -5 days, the column drying intensifies

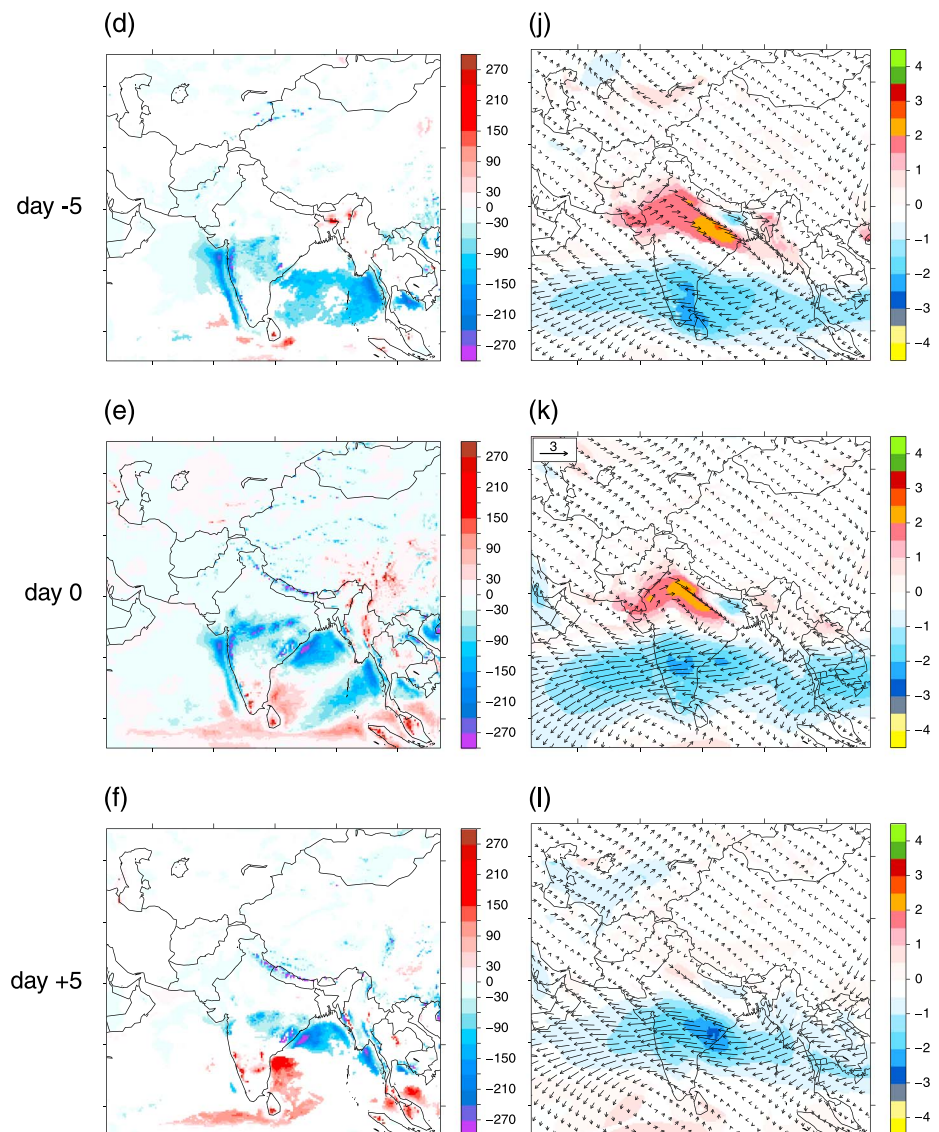


Figure 6. (continued)

along with development of cold temperature anomalies that peak around 600–500 hPa (Figure 8c), just around the 0°C isotherm layer (Figure 3d). The combined cold and dry air increases the stability of the atmospheric column, a factor that arrests the development of cumulus convection. These conditions amplify and persist during the peak break phase at day 0. The baroclinic vertical structure in temperature anomalies at day 0 is a consequence of reduced convective heating at midlevels and hence reduced evaporative cooling due to downdraft in the lower troposphere. Furthermore, cloud-free conditions during breaks promote stronger shortwave heating at the surface, whereas less trapping of upwelling radiation leads to a stronger radiative cooling, and therefore stronger descent and drying of the atmospheric column. The HIRHAM5 temperature profile broadly agrees with high-resolution radiosonde observations over the north Bay of Bengal during break monsoon conditions [Bhat et al., 2002]. In summary, the modeled vertical profiles of key variables that signify stability in the atmospheric column correspond reasonably well with available observations or reanalysis products [Prasanna and Annamalai, 2012], but the simulated amplitudes are weaker by 50–80% (not shown). The implication is that the simulated intensity of breaks over central India is weaker than observed.

Despite the above model deficiencies in the representation of the basic state and its dominant mode of variability, HIRHAM5 demonstrates ability in simulating the leading processes that account for monsoon breaks.

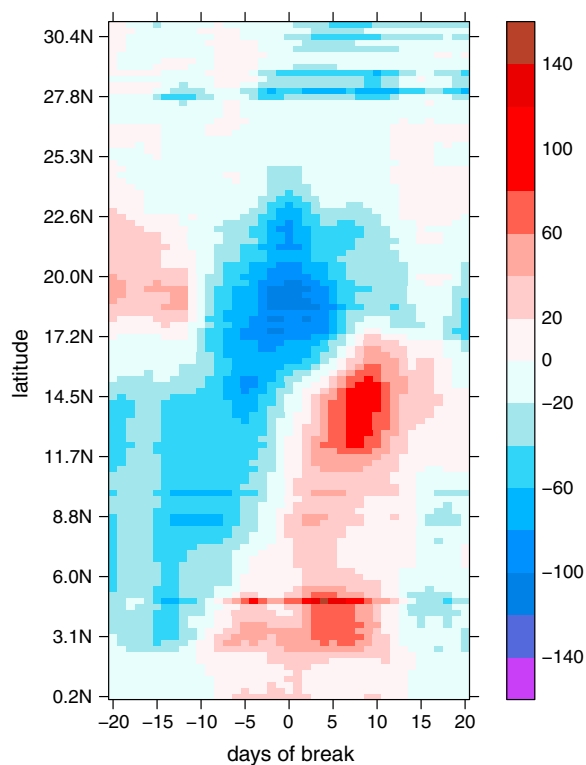


Figure 7. Latitude-time lag plot of 70°–90°E averaged precipitation anomalies (W m^{-2}) during the life cycle of breaks (from days –20 to days +20). Day 0 refers to the peak phase of monsoon breaks and maximum amplitude of rainfall anomalies over central India.

As the next section will show, MSE analysis helps to identify these processes and quantify their relative contributions, and by comparing model results with reanalysis products aid to bring out model shortcomings.

5. HIRHAM5 MSE Budget

This section addresses the representation of physical processes in HIRHAM5 during breaks and quantifies the relative contributions of the competing moist and radiative processes in causing anomalous rainfall over central India. As mentioned earlier, vertical advection of anomalous MSE is directly proportional to precipitation anomalies and thus aids in the interpretation of other MSE terms in anchoring the precipitation anomalies. In the following, for enhanced resolution in the troposphere and stratosphere, the quantitative diagnostics of the MSE budget are performed on a new interpolated (from the original 40 model level) set of 32-level HIRHAM5 pressure data, instead of using 15-level HIRHAM5 pressure data, as recommended by *Trenberth et al.* [2002] for reanalysis data.

To infer the origin of anomalous thermodynamic conditions leading to breaks over central India, Figure 9 shows spatial evolution of vertically integrated anomalous model DSE (a–f) and MSE (g–l) for –20 days to +5 days, respectively. Different patterns in the sign of DSE and MSE anomalies over India demonstrate that also in HIRHAM5 primarily moisture related processes regulate MSE anomalies in the deep tropics. Compared to anomalous precipitation evolution (Figure 6a–6f) buildup of negative MSE anomalies begins over northwest India around day –15 (Figure 9h) and continues to amplify thereafter. While at day 0, DSE shows a maximum positive anomaly over central India (Figure 9e), and MSE anomalies are negative in sign there (Figure 9k). Our interpretation is that column-integrated DSE anomalies appear to be a response, while MSE anomalies are a precursor to precipitation anomalies. Vertical plots over central India (Figure 10) show that DSE anomalies are almost entirely regulated by temperature anomalies (Figures 8c and 10a), while MSE anomalies grow in association with specific humidity anomalies (Figures 8b and 10b). Note that the amplitude of temperature (DSE) anomalies are much weaker compared to variations in specific humidity (MSE), implying the dominant role of moisture anomalies in the evolution of breaks. Over central India, the intense low-level warming (Figure 8c) leads to an increase in DSE (Figure 10a) and dominates the column-averaged DSE at day 0 (Figure 9e).

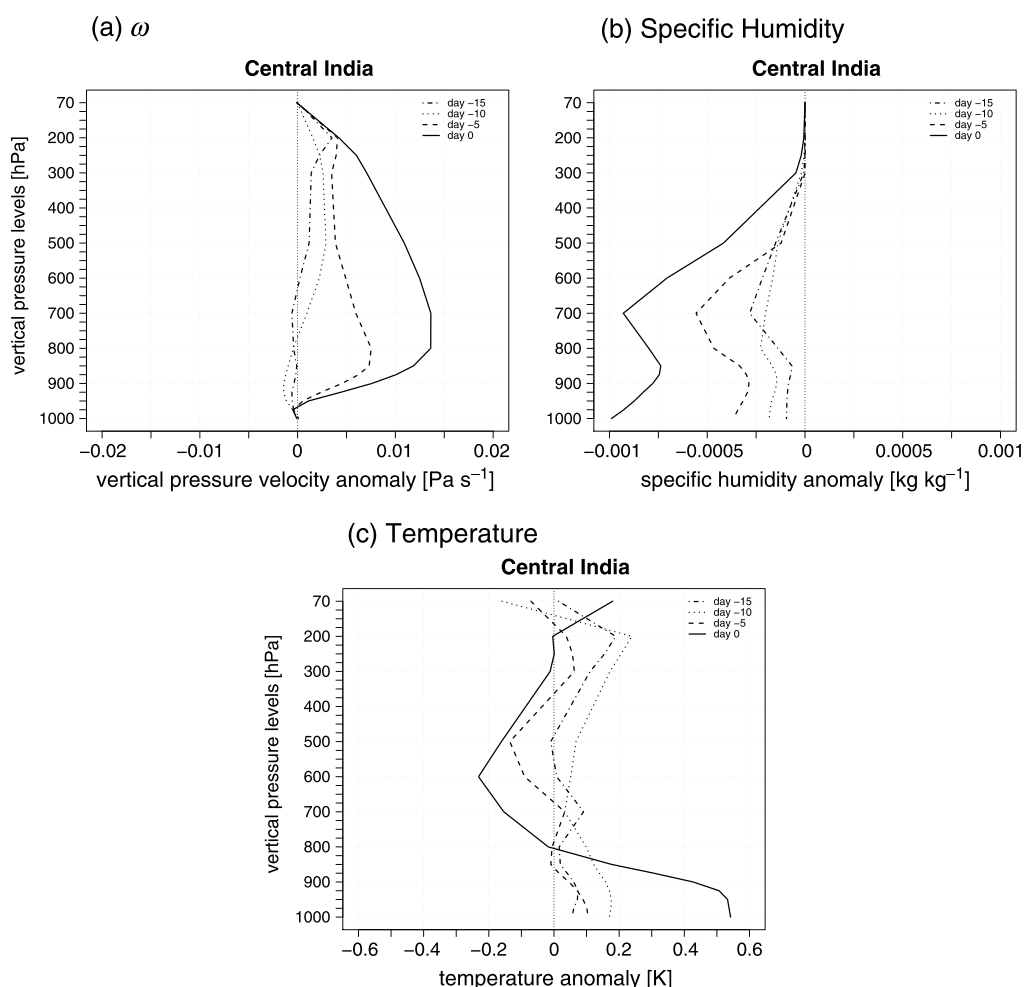


Figure 8. Vertical distribution of composite anomalies for (a) vertical pressure velocity ω (Pa s^{-1}), (b) specific humidity (kg kg^{-1}), and (c) temperature ($^{\circ}\text{C}$) averaged over central India (21° – 27°N , 72° – 85°E) from HIRHAM5. The composites are shown from days -15 to day 0 .

During the onset of breaks, the column-integrated model MSE is governed by middle to lower tropospheric MSE discharge over central India with maximum negative MSE anomalies peak at around 700 hPa (Figure 10b) corresponding to the level of maximum negative specific humidity anomalies (Figure 8b). While the low-level MSE anomalies are almost entirely controlled by moisture, upper level MSE anomalies are mainly governed by temperature variations.

Figure 11 compares the temporal evolution of all budget terms over central India constructed from HIRHAM5 (a) with that from ERA-Interim (b) from -20 days to $+15$ days of the break cycle. To aid in their interpretation, Figure 11 also shows the anomalous precipitation whose units are shown on the right-hand side ordinate. Positive (negative) values of vertical MSE advection mean energy export (import) in the atmospheric column. A positive (negative) sign of net radiative flux represents a total radiative warming (cooling) of the column, and moist (dry) advection into the column is positive (negative) in sign. As in ERA-Interim, the MSE tendency term (pink curve) closely follows the moisture advection term (red curve) with discharge of MSE occurring before break phase and recharge of MSE occurring during and after breaks, indicating anomalous dry (moist) advection as a key moist process in initiating (terminating) breaks over central India. Although the model captures the temporal evolution of MSE tendency and moisture advection, their amplitudes are reduced compared to ERA-Interim diagnostics during breaks. Budget studies with different reanalysis indicate proportionality between the import of MSE (MSE divergence) and precipitation anomalies [Kiranmayi and Maloney, 2011; Prasanna and Annamalai, 2012]. However, in the model, negative MSE convergence (light blue curve) and negative rainfall anomalies (dashed blue curve) seem to be out of phase by 3 days, with a

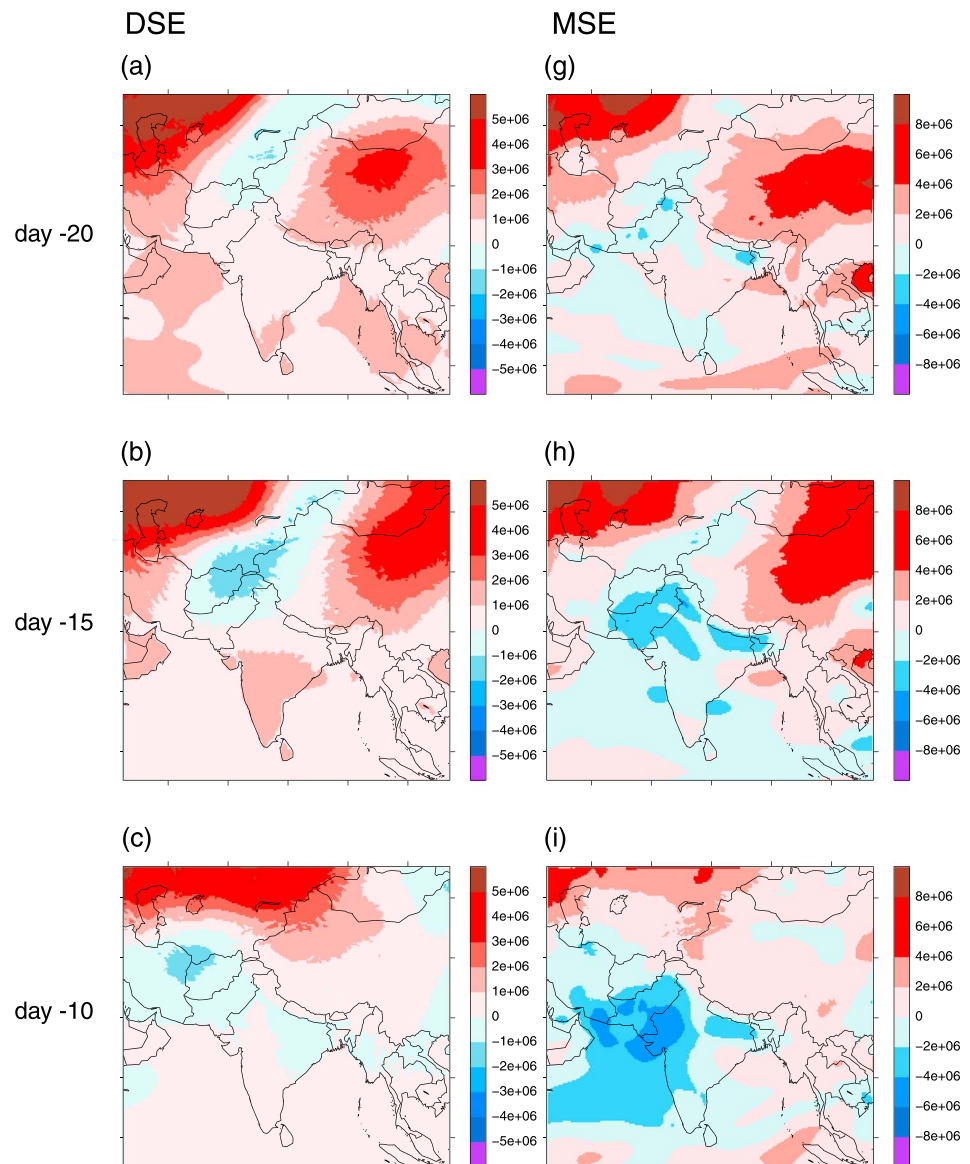


Figure 9. Space-time evolution of composite anomalies of (a–f) vertically integrated DSE (W m^{-2}) and (g–i) vertically integrated MSE (W m^{-2}) during breaks. The composites are shown from days -20 to days $+5$ with day 0 defined as the peak phase of monsoon breaks and maximum amplitude of rainfall anomalies. Each panel is 5 days apart.

“peak” MSE divergence at approximately day -3 and compared to ERA-Interim, model values are reduced by a factor of ~ 5 . During the entire life cycle of breaks, the contribution from vertical advection of MSE (light blue curve) is smaller than its horizontal counterpart (not shown) including horizontal temperature advection (green curve) and horizontal moisture advection (red curve) in HIRHAM5, a feature also noted in diagnostics of the Community Atmospheric Model version 3 during MJO events [Maloney, 2009]. Consistent with the ERA-Interim budget, the contribution from evaporation (orange curve) is small. The surface sensible heat flux (purple curve) increases due to rather cloud-free conditions indicated by the lack of rainfall (Figures 6d–6f) over central India from day -5 onward, but with twice the amplitude of ERA-Interim in HIRHAM5 (Figures 11a and 11b). Radiative cooling is primarily responsible for the persisting negative MSE convergence and rainfall anomalies in reanalysis budget diagnostics [Prasanna and Annamalai, 2012]. While HIRHAM5 captures the net radiative cooling (gray curve) contributions with a similar order of magnitude as ERA-Interim during breaks, negative MSE convergence and rainfall anomalies are simulated too small in the model.

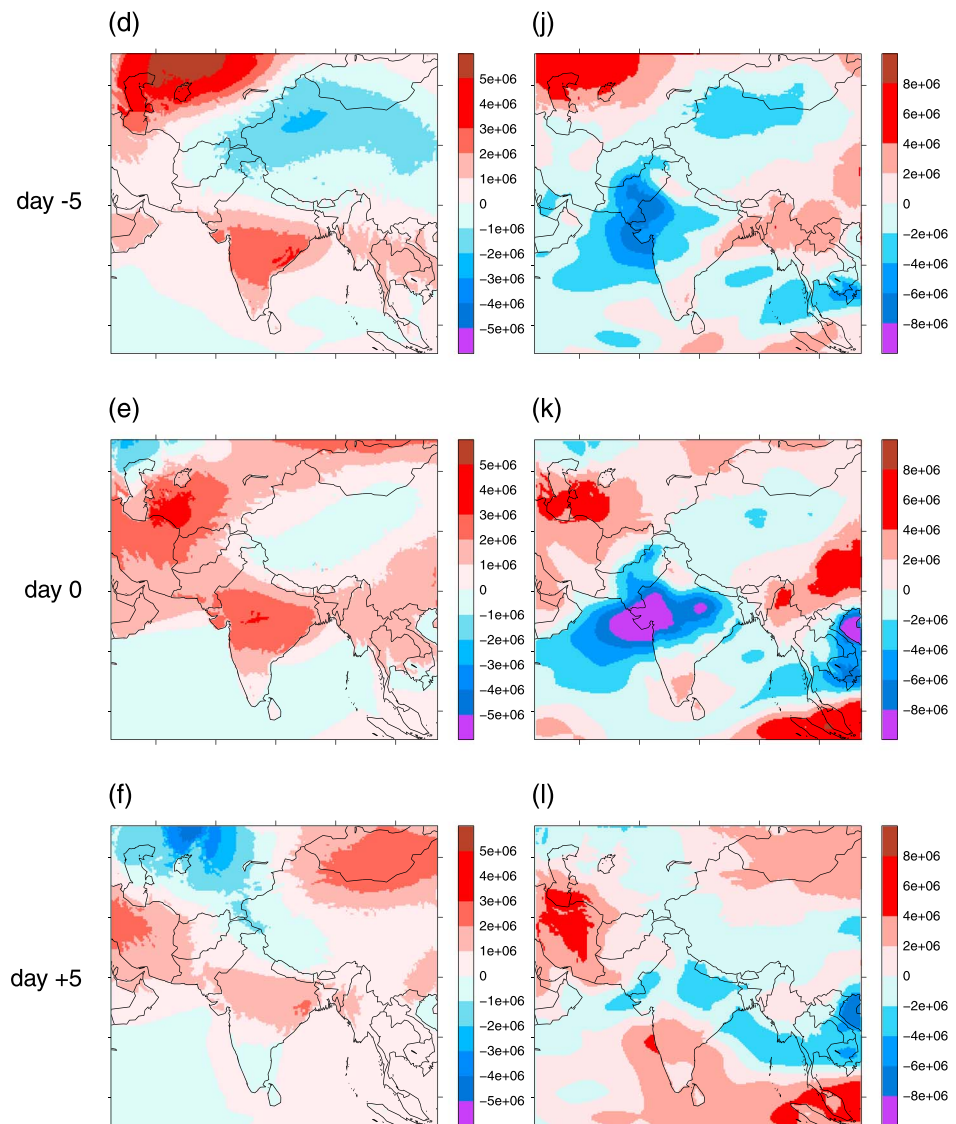


Figure 9. (continued)

Further, it should be noted that a considerable residual term with amplitudes as large as and with similar behavior to the MSE tendency term appears in both the HIRHAM5 and the ERA-Interim budget (Figures 11a and 11b, black dashed curve), but with smaller values for the model data compared to the reanalysis. Residuals have also been found in other MSE budget studies based on reanalysis data [Back and Bretherton, 2006; Kiranmayi and Maloney, 2011; Prasanna and Annamalai, 2012]. Kiranmayi and Maloney [2011] attributed these residuals to missing or miscalculating MSE sources in the moist physics of the reanalysis model (e.g., shallow convection). In addition, Prasanna and Annamalai [2012] proposed that interpolations from native model coordinates to standard pressure levels, and the fact that the vertically integrated MSE budget equation itself arises due to cancellation of large terms (namely, convective heating and moisture sink in the dry thermodynamic equation and moisture equation) will introduce residuals of uncertain sign. Further, neglecting horizontal diffusion in the horizontal advection terms could be a source of residuals. Overall, the existence of a residual term in HIRHAM5 poses clearly a caveat for the model results of the break analysis in the present study.

To better understand the model shortcomings associated with the net radiative flux term into the column, we now consider the temporal evolution of the balance between the individual terms of the anomalous net radiative flux at the surface (a/c) and at the top of the atmosphere (TOA) (b/d) during breaks for HIRHAM5/ERA-Interim in Figure 12. The net sum of absorbed shortwave radiation fluxes and downward longwave

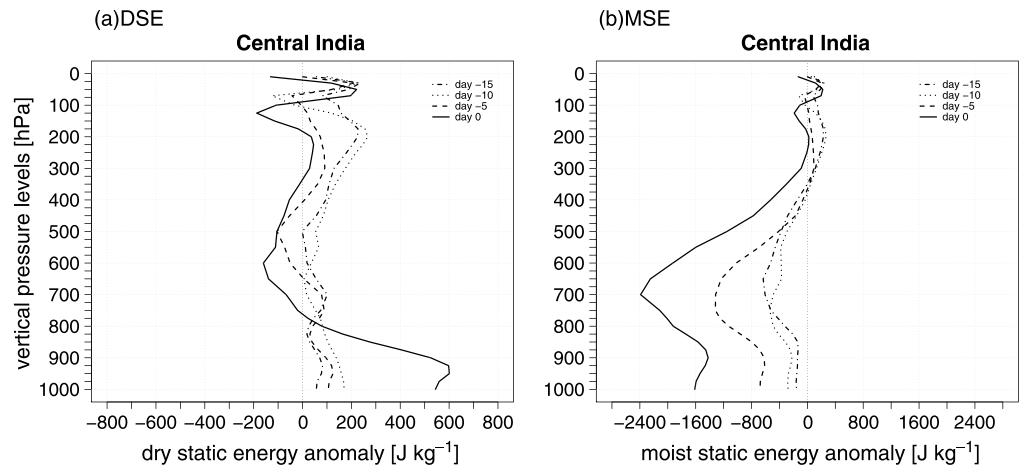


Figure 10. Vertical distribution of composite anomalies for (a) DSE (J kg^{-1}) and (b) MSE (J kg^{-1}) averaged over central India (21° – 27°N , 72° – 85°E) from HIRHAM5. The composites are shown from days –15 to day 0.

radiation fluxes at the surface is defined as the surface heating [Prasanna and Annamalai, 2012]. Cloud-free conditions during breaks promote more shortwave to reach the surface followed by an increased upwelling of shortwave and longwave radiation. In response, radiative cooling increases, and to compensate this cooling, adiabatic descent increases which in turn inhibits cloud growth and promotes maintenance of breaks. The temporal evolution of the surface energy budget terms from HIRHAM5 capture the features noted in ERA-Interim, but the model simulates stronger shortwave radiation reaching the surface during breaks (Figures 12a and 12c). Wild and Roeckner [2006] found systematically underestimated atmospheric shortwave absorption along with overestimated surface shortwave absorption at low latitudes in ECHAM5 and related these errors to the crude aerosol climatology used in the physical parameterization package, which does not take into account high regional and seasonal loadings of absorbing aerosols. During the past few decades, direct surface radiation measurements observed continuous and steady dimming in India associated with tremendous aerosol emissions due to rapid urbanization and population growth [Wild et al., 2009], and more recent studies with satellite observations noticed increased aerosol loadings over central India especially during break conditions [e.g., Manoj et al., 2012; Bhawar and Rahul, 2013]. Since the ECHAM5 aerosol climatology is also implemented in HIRHAM5, we assume that anomalous high-simulated incoming surface shortwave radiation flux during breaks is perhaps partly due to weak atmospheric aerosol absorption. The TOA energy

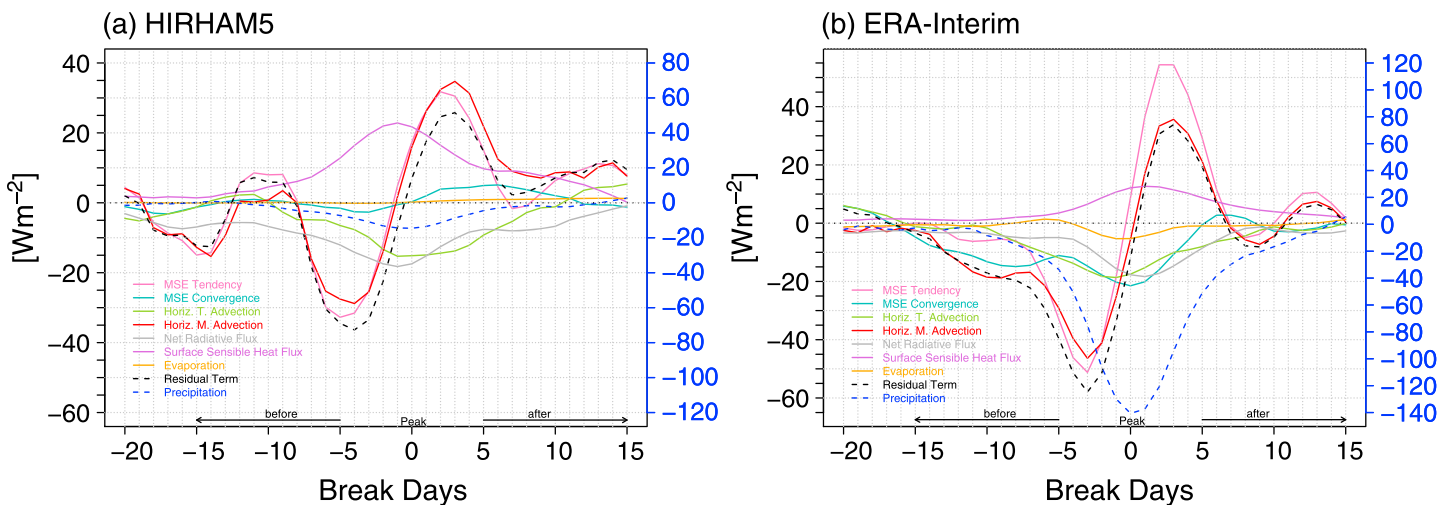


Figure 11. Composite temporal evolution of individual terms of the MSE budget averaged over central India (21° – 27°N , 72° – 85°E) from (a) HIRHAM5 and (b) ERA-Interim. All units are in W m^{-2} , and the time evolution is from left to right (–20 days to +15 days). Note that the units for the dashed lines (residual term and precipitation) are shown on the right-hand side ordinate.

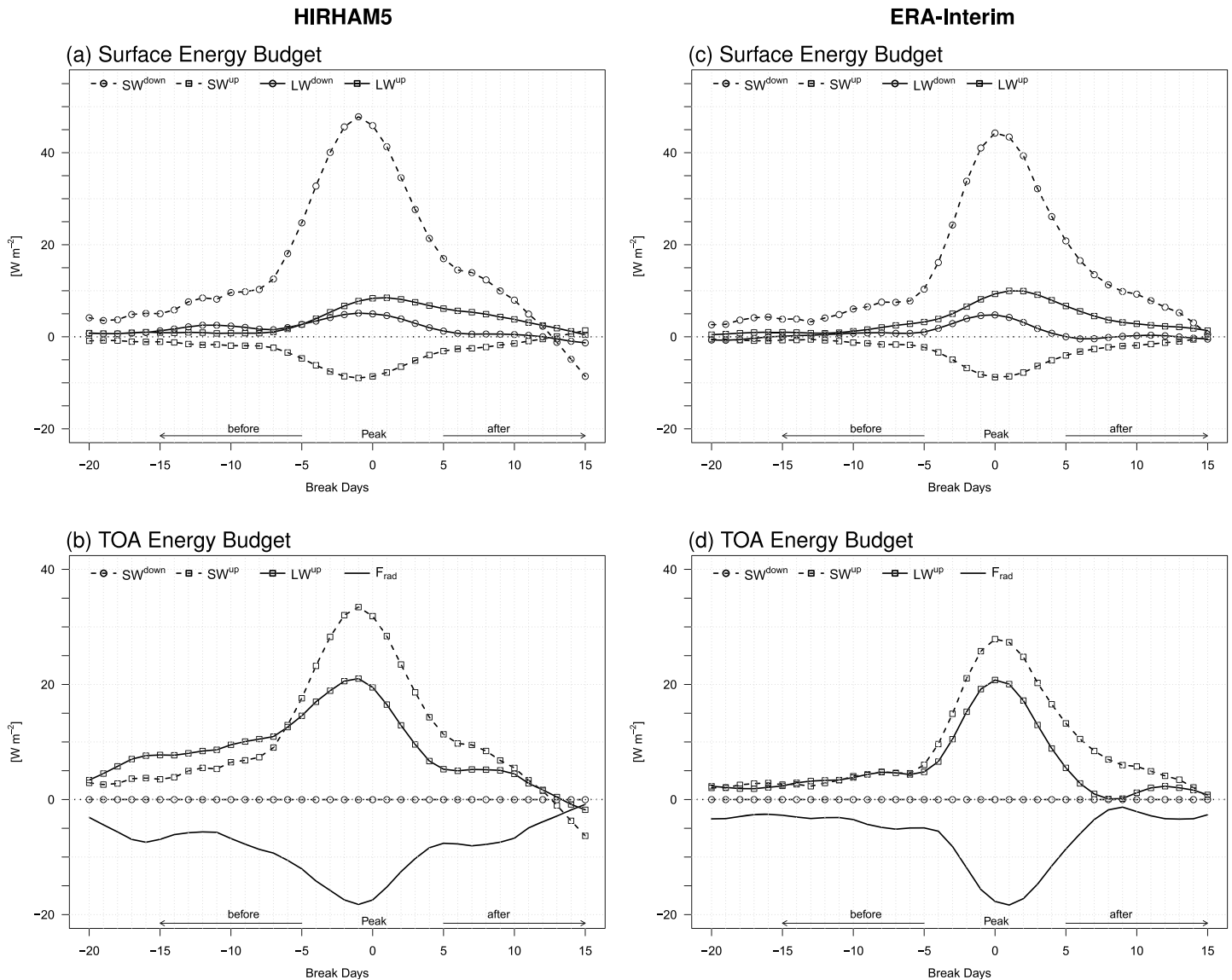


Figure 12. Composite temporal evolution of individual terms of (a, c) the surface energy budget and (b, d) the TOA (top of the atmosphere) energy budget during breaks for HIRHAM5/ERA-Interim averaged over central India (21°–27°N, 72°–85°E). All units are in $W m^{-2}$. The composites are shown from days –20 to day +15. Dashed (solid) line represents shortwave (longwave) component, while open squares (circles) show upward (downward) fluxes, respectively.

budget represents the energy input to the atmospheric column. The prevailing balance between net radiative cooling and both enhanced outgoing longwave and shortwave radiation during breaks in the reanalysis data (Figure 12d) is also captured by HIRHAM5 (Figure 12b). However, the model simulates too high anomalous outgoing shortwave radiation fluxes during breaks and a delayed return to around zero anomalies of outgoing longwave radiation fluxes after the break, which results in a too persistent net radiative cooling over central India from +5 to +10 days (Figure 12b). Given that especially in the tropics, there is a direct proportionality between convective activity and net tropospheric energy input from surface fluxes and radiation [Raymond, 2001], the inconsistent development of the precipitation term and the net radiative flux term in HIRHAM5 during the break cycle (the negative precipitation anomalies should be ~6 times the amount of net radiative cooling) reveals a shortcoming in the moisture-radiation interaction in HIRHAM5.

6. Summary and Discussion

6.1. Summary

In this study the performance of the RCM HIRHAM5, driven by the ERA-Interim reanalysis data in simulating monsoon breaks over India, as a part of the BSISV is examined with focus on moist and radiative processes.

Since the MSE represents a quantity linking physical processes influencing moisture and temperature, the vertically integrated MSE budget was used as an approach to understand the representation of the physical parameterization (diabatic sources) and dynamical core (adiabatic terms) of the RCM.

In the monsoon basic state, HIRHAM5 captures observed orographically induced heavy precipitation surrounding continental India (foothills of the Himalayas, along the Western Ghats, the Arakan Range, and Tenasserim Range in Burma). However, model deficiencies include a dry and warm bias over northwest and central India, and excess rainfall over the open oceans of the southern Bay of Bengal and near-equatorial Arabian Sea. It is found that similar precipitation biases are also present in ERA-Interim but of weaker magnitude. This allowed us to suggest that a part of the model bias could originate from the driving data. A comparison of ω profiles with reanalysis revealed a too strong uplift in the upper to midtroposphere along with an overly top-heavy structure over the Bay of Bengal in HIRHAM5, whereas anomalous climatological descent is simulated throughout the free troposphere over central India. Based on these biases, we hypothesized the following mechanism for the dry bias over central India: Excess rainfall over the southern Bay of Bengal forces near-equatorial Rossby wave response with anomalous descent over continental India (validated by performing idealized numerical experiments, Figures 4a and 4b). Additionally, positive rainfall anomalies over the near-equatorial Arabian Sea and Bay of Bengal anchor a local Hadley-type circulation that promotes descent anomalies over the Indian continent (validated by estimating the local Hadley-type circulation bias of the mass flux and stream function averaged over the Indian longitudes 68°–96°E in HIRHAM5, Figure 5). Both mechanisms support our interpretation, which excess rainfall over the ocean regions promotes anomalous climatological descent over central India leading to the dry bias in CWV, specific humidity, and rainfall.

Breaks over India were investigated following the method used by *Prasanna and Annamalai* [2012]. It was found that HIRHAM5 demonstrates ability in representing the observed northward progression of negative rainfall anomalies over the Indian longitudes, representing the 40 day intraseasonal mode. It is shown that the model simulates the break phase lasting for at least 10 days over central India, but of weaker intensity compared to observations. Temporal changes of the atmospheric stability over central India in association with monsoon breaks are found to be in good agreement with observations and reanalysis data. This consensus encouraged us to diagnose column-integrated MSE budgets over central India during the life cycle of breaks. The budget analysis indicated that in the model too, anomalous dry advection is a key process in initiating, while net radiative cooling is the leading process in maintaining monsoon breaks. However, quantitatively, all diabatic terms of the HIRHAM5 MSE budget were found to be weaker in amplitudes compared to reanalysis diagnostics, and especially, the MSE divergence term seems to be -3 day out of phase and reduced by factor of ~ 5 (Figure 11). An examination of the net radiative balance at the surface revealed a too strong simulated shortwave downwelling radiation flux. Already detected shortcomings in the aerosol climatology of the physical parameterization package of ECHAM5 [*Wild and Roeckner*, 2006], which is also incorporated in the HIRHAM5 physics, allowed us to assume that anomalous high-simulated shortwave surface income during cloud-free conditions of breaks can be partly attributed to weak atmospheric aerosol absorption.

6.2. Discussion

Indian summer monsoon rainfall produced in climate models is sensitive to the cumulus parameterization scheme used [e.g., *Mukhopadhyay et al.*, 2010; *Srinivas et al.*, 2012; *Sinha et al.*, 2013]. A comparison between the simulated convective and large-scale part of the total monsoon precipitation in HIRHAM5 (Figures 13a and 13b) reveals that the total precipitation bias primarily results due to model deficiencies in the simulation of the convective precipitation. Dry (wet) bias in convective rainfall over most parts of continental India (the southern Bay of Bengal and southeastern Arabian Sea) is in line with the detected biases in total precipitation (Figures 1a and 1b).

As one last note, Figure 14 shows the simulated relationship between monthly mean CWV and precipitation compared to ERA-Interim for the two regions of interest: central India (a) and Bay of Bengal (b). For both regions, all JJAS months in 1979–2012 at all locations were stratified into 1 mm CWV bins. While over central India, HIRHAM5 simulates too less rainfall for the same amount of CWV (for CWV > 30 mm) compared to the reanalysis, the model is overreacting for the moist, heavily precipitating bins (for CWV > 54 mm) and simulates excess rainfall over Bay of Bengal. In other words, the relationship between a given CWV and the simulated precipitation over central India is systematically too low in the model, suggesting shortcomings in the cloud microphysics. In contrast over the Bay of Bengal, the monotonous increase in precipitation with

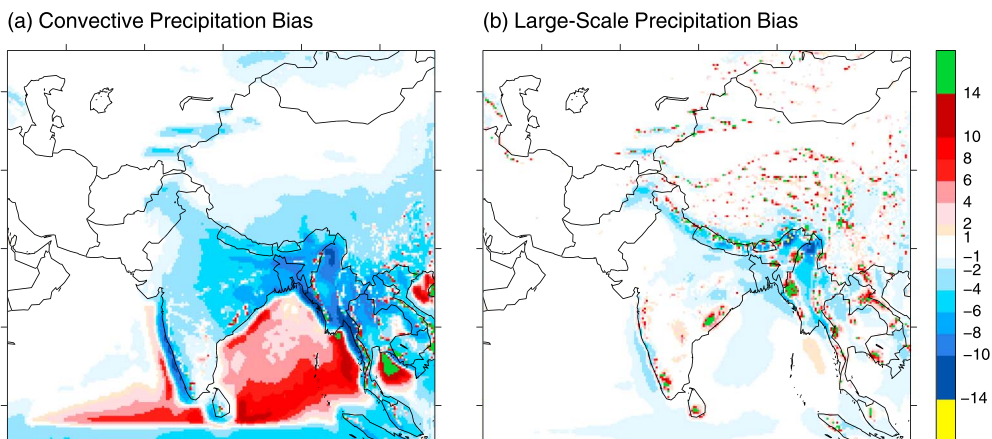


Figure 13. June–September averaged (a) convective and (b) large-scale precipitation bias (mm d^{-1}) with respect to ERA-Interim (1979–2012).

CWV suggests that deep convection is too predominant in the model resulting in overly simulated top-heavy ω structure (Figure 3b). Given the fact that the SST employed as boundary condition in HIRHAM5 is taken from ERA-Interim, the excessive simulations of CWV (Figure 2b) and rainfall (Figure 1a) over the Bay of Bengal, and the sensitive of precipitation to CWV (Figure 14), suggest deficiencies in HIRHAM5’s precipitation formation over tropical oceans. Overestimated shortwave cloud forcing in the intertropical convergence zone ocean regions during boreal summer found in ECHAM5 [Wild and Roeckner, 2006] is consistent with enhanced rainfall in these regions in HIRHAM5.

Given that the aim of this study has been the examination of HIRHAM5’s fidelity to simulate monsoon breaks as a feature of the BSISV, we have investigated the model’s monsoon basic state as a necessary condition for a realistic representation of intraseasonal monsoon variability. We conclude that if ERA-Interim is realistic, then diagnostics presented here identify limitations in the model simulation setup used, and therefore, “downscaling” offers a test bed for RCM evaluation. We found that HIRHAM5 demonstrates ability in capturing regional features of monsoon breaks and is therefore suitable for regional monsoon prediction and future climate change projections. Yet the reasons for the model’s overreacting behavior for high CWV and the weak representation of moisture-radiation interactions are not seen and have to be addressed in future investigations. For instance, it is unclear if the model setup has not been suitably selected. To understand the origin of the precipitation bias (especially the convective precipitation bias and its sensitivity to CWV), detailed process-oriented diagnostics including that of microphysics and sensitivity studies are needed. Having recognized that realistic simulation of the basic state is a “zeroth order” requirement in models, our future research will focus on the convection scheme, the sensitivity with respect to the lateral and lower boundary driving

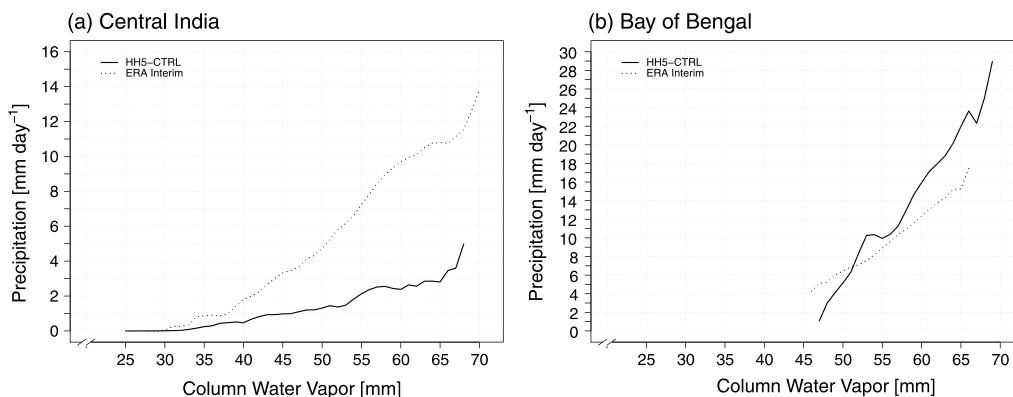


Figure 14. Mean monthly averaged precipitation (mm d^{-1}) in 1 mm wide bins of column water vapor (mm), for (a) the central India (21° – 27°N , 72° – 85°E) and (b) for the Bay of Bengal (7° – 15°N , 87° – 101°E) region from HIRHAM5 (solid line) and ERA-Interim (dashed line) for all June–September months in 1979–2012.

data, the model domain (in particular the placement of the southern boundary), and the buffer zone size of the boundary relaxation method. This will help to eliminate their contribution to the precipitation bias. A direct implication of our results is that more diagnostics are necessary, apart from just investigating the northward propagation feature to verify the ability of a RCM to represent BSISV.

Acknowledgments

The authors sincerely thank Walter Hannah for thoughtful and constructive comments and critics that improved the manuscript significantly. The authors also acknowledge the other anonymous reviewer whose comments helped in the improvement. This study was partially conducted in the Graduate School GRK1364 "Interactions between tectonics, climate, and the biosphere in the African-Asian monsoonal region" funded by the German Research Foundation (DFG), cofinanced by the federal state of Brandenburg and the University of Potsdam. This work was also supported by the IPRC. H. Annamalai and Franziska S. Hanf acknowledge partial support from NSF (grant 1460742). The simulation with the HIRHAM5 was performed at the German Climate Computing Center (DKRZ, Hamburg). For data access, please contact fhanf@hawaii.edu. The authors thank the ECMWF for providing the ERA-Interim product that made this study possible, Ines Hebestadt for technical support with setting up the HIRHAM5 simulation, Jan Hafner for the help in running the LBM experiments, and Mohana S. Thota for providing the codes to estimate the budget diagnostics. The APHRODITE precipitation data were freely obtained from the APHRODITE's Water Resources project (<http://www.chikyuu.ac.jp/precip/english/products.html>). The TRMM satellite data are freely available from the NASA/Goddard Space Flight Center's Mesoscale Atmospheric Processes Laboratory and PPS (ftp://disc2.nascom.nasa.gov/data/TRMM/Gridded/Derived_Products/3B42_V7/Daily/). This paper is IPRC/SOEST contribution 1249/10001.

References

- Ajayamohan, R. S., H. Annamalai, J. J. Luo, J. Hafner, and T. Yamagata (2011), Poleward propagation of boreal summer intraseasonal oscillations in a coupled model: Role of internal processes, *Clim. Dyn.*, *37*, 851–867, doi:10.1007/s00382-010-0839-6.
- Andersen, J. A., and Z. Kuang (2012), Moist static energy budget of MJO-like disturbances in the atmosphere of a zonally symmetric aquaplanet, *J. Clim.*, *25*, 2782–2804.
- Annamalai, H. (2010), Moist dynamical linkage between the equatorial Indian Ocean and the South Asian Monsoon trough, *J. Atmos. Sci.*, *67*, 589–610.
- Annamalai, H., and J. M. Slingo (2001), Active/break cycles: Diagnosis of the intraseasonal variability of the Asian Summer Monsoon, *Clim. Dyn.*, *18*, 85–102.
- Annamalai, H., and K. R. Sperber (2005), Regional heat sources and the active and break phases of boreal summer intraseasonal (30–50 day) variability, *J. Atmos. Sci.*, *62*, 2726–2748.
- Annamalai, H., J. M. Slingo, K. R. Sperber, and K. Hodges (1999), The mean evolution and variability of the Asian Summer Monsoon: Comparison of ECMWF and NCEP-NCAR reanalyses, *Mon. Weather Rev.*, *127*, 1157–1186.
- Back, L. E., and C. S. Bretherton (2006), Geographic variability in the export of moist static energy and vertical motion profiles in the tropical Pacific, *Geophys. Res. Lett.*, *33*, L17810, doi:10.1029/2006GL026672.
- Befort, D. J., G. C. Leckebusch, and U. Cubasch (2016), Intraseasonal variability of the Indian summer monsoon: Wet and dry events in COSMO-CLM, *Clim. Dyn.*, *47*, 2635–2651, doi:10.1007/s00382-016-2989-7.
- Bhat, G. S., A. Chakraborty, R. S. Nanjundiah, and J. Srinivasan (2002), Vertical thermal structure of the atmosphere during active and weak phases of convection over the north Bay of Bengal: Observation and model results, *Curr. Sci.*, *83*(3), 296–302.
- Bhawar, R. L., and P. R. C. Rahul (2013), Aerosol-cloud-interaction variability induced by atmospheric brown clouds during the 2009 Indian summer Monsoon Drought, *Aerosol Air Qual. Res.*, *13*(4), 1384–1391.
- Boos, W. R., and J. V. Hurlley (2013), Thermodynamic bias in the multimodel mean boreal summer monsoon, *J. Clim.*, *26*, 2279–2287.
- Boos, W. R., and Z. Kuang (2010), Mechanisms of poleward propagating, intraseasonal convective anomalies in cloud system-resolving models, *J. Atmos. Sci.*, *67*, 3673–3691.
- Christensen, O. B., M. Drews, J. H. Christensen, K. Dethloff, K. Ketelsen, I. Hebestadt, and A. Rinke (2007), The HIRHAM regional climate model version 5 (β), *Tech. Rep. (06-17)*, 22 pp., Danish Meteorol. Inst., Copenhagen, Denmark.
- Dash, S. K., A. Mamgain, K. Pattanayak, and F. Giorgi (2012), Spatial and temporal variations in Indian summer monsoon rainfall and temperature: An analysis based on RegCM3 Simulations, *Pure Appl. Geophys.*, *170*(4), 655–674.
- Davies, H. C. (1976), A lateral boundary formulation for multi-level prediction models, *Q. J. R. Meteorol. Soc.*, *102*, 405–418.
- Davies, H. C., and R. E. Turner (1977), Updating prediction models by dynamical relaxation: An examination of the technique, *Q. J. R. Meteorol. Soc.*, *103*, 225–245.
- Dee, D. P., et al. (2011), The ERA-Interim reanalysis: Configuration and performance of the data assimilation system, *Q. J. R. Meteorol. Soc.*, *137*, 553–597, doi:10.1002/qj.828.
- Dobler, A., and B. Ahrens (2010), Analysis of the Indian summer monsoon system in the regional climate model COSMO-CLM, *J. Geophys. Res.*, *115*, D16101, doi:10.1029/2009JD013497.
- Fouquart, Y., and B. Bonnel (1980), Computations of solar heating of the Earth's atmosphere: A new parameterization, *Contrib. Atmos. Phys.*, *53*, 35–62.
- Gill, A. E. (1980), Some simple solutions for heat-induced tropical circulation, *Q. J. R. Meteorol. Soc.*, *106*, 447–462.
- Gollvik, S. (1999), On the effects of horizontal diffusion, resolution and orography on precipitation forecasting in a limited area model, *Meteorol. Appl.*, *6*, 49–58.
- Hagemann, S. (2002), An improved land surface parameter dataset for global and regional climate models, *Tech. Rep. 336*, 28 pp., Max Planck Inst. for Meteorol., Hamburg, Germany.
- Hagemann, S., K. Arpe, and E. Roeckner (2006), Evaluation of the hydrological cycle in the ECHAM5 model, *J. Clim.*, *19*, 3810–3827, doi:10.1175/JCLI3831.1.
- Hannah, W. M., and E. D. Maloney (2011), The role of moisture–convection feedbacks in simulating the Madden–Julian Oscillation, *J. Clim.*, *24*, 2754–2770.
- Huffman, G. J., R. F. Adler, D. T. Bolvin, G. Gu, E. J. Nelkin, K. P. Bowman, Y. Hong, E. F. Stocker, and D. B. Wolff (2007), The TRMM Multisatellite Precipitation Analysis (TMPA): Quasi-global, multiyear, combined-sensor precipitation estimates at fine scales, *J. Hydrometeorol.*, *8*, 38–55, doi:10.1175/JHM560.1.
- Kiranmayi, L., and E. D. Maloney (2011), Intraseasonal moist static energy budget in reanalysis data, *J. Geophys. Res.*, *116*, D21117, doi:10.1029/2011JD016031.
- Klaus, D., K. Dethloff, W. Dorn, A. Rinke, and D. L. Wu (2016), New insight of Arctic cloud parameterization from regional climate model simulations, satellite-based, and drifting station data, *Geophys. Res. Lett.*, *43*, 5450–5459, doi:10.1002/2015GL067530.
- Krishnan, R., C. Zhang, and M. Sugi (2000), Dynamics of breaks in the Indian Summer Monsoon, *J. Atmos. Sci.*, *57*, 1354–1372.
- Lohmann, U., and E. Roeckner (1996), Design and performance of a new cloud microphysics scheme developed for the ECHAM general circulation model, *Clim. Dyn.*, *12*(8), 557–572, doi:10.1007/BF00207939.
- Lucas-Picher, P., J. H. Christensen, F. Saeed, P. Kumar, S. Asharaf, B. Ahrens, A. J. Wiltshire, D. Jacob, and S. Hagemann (2011), Can regional climate models represent the Indian Monsoon?, *J. Hydrometeorol.*, *12*, 849–868.
- Maloney, E. D. (2009), The moist static energy budget of a composite tropical intraseasonal oscillation in a climate model, *J. Clim.*, *22*, 711–729.
- Manoj, M. G., P. C. S. Devara, S. Joseph, and A. K. Sahai (2012), Aerosol indirect effect during the aberrant Indian Summer Monsoon breaks of 2009, *Atmos. Environ.*, *60*, 153–163.
- Mlawer, E. J., S. J. Taubman, P. D. Brown, M. J. Iacono, and S. A. Clough (1997), Radiative transfer for inhomogeneous atmospheres: RRTM, a validated k-correlated model for the longwave, *J. Geophys. Res.*, *102*, 16,663–16,682.

- Mukhopadhyay, P., S. Taraphdar, B. N. Goswami, and K. Krishnakumar (2010), Indian Summer Monsoon precipitation climatology in a high-resolution regional climate model: Impacts of convective parameterization on systematic biases, *Weather Forecasting*, *25*, 369–387, doi:10.1175/2009WAF2222320.1.
- Nordeng, T. E. (1994), Extended versions of the convective parametrization scheme at ECMWF and their impact on the mean and transient activity of the model in the tropics, *Tech. Memo. (206)*, 41 pp., European Centre for Medium-Range Weather Forecasts, Reading, U. K.
- Polanski, S., A. Rinke, and K. Dethloff (2010), Validation of the HIRHAM-simulated Indian summer monsoon circulation, *Adv. Meteorol.*, *2010*, 415632, doi:10.1155/2010/415632.
- Prasanna, V., and H. Annamalai (2012), Moist dynamics of extended monsoon breaks over South Asia, *J. Clim.*, *25*(11), 3810–3831.
- Raghavan, K. (1973), Break-Monsoon over India, *Mon. Weather Rev.*, *101*(1), 33–43.
- Rajendran, K., A. Kitoh, J. Srinivasan, R. Mizuta, and R. Krishnan (2012), Monsoon circulation interaction with Western Ghats orography under changing climate, *Theor. Appl. Climatol.*, *110*, 555–571.
- Ramamurthy, K. (1969), Monsoons of India: Some aspects of the 'break' in the Indian southwest monsoon during July and August, Forecasting Manual, PART 4 (18.3), India Meteorol. Dep., Poona, India.
- Raymond, D. J. (2001), A new model of the Madden–Julian oscillation, *J. Atmos. Sci.*, *58*, 2807–2819.
- Raymond, D. J., S. L. Sessions, A. H. Sobel, and Ž. Fuchs (2009), The mechanics of gross moist stability, *J. Adv. Model. Earth Syst.*, *1*, 9, doi:10.3894/JAMES.2009.1.9.
- Rodwell, M. J., and B. J. Hoskins (1996), Monsoons and the dynamics of deserts, *Q. J. R. Meteorol. Soc.*, *122*, 1385–1404.
- Roeckner, E., et al. (2003), The atmospheric general circulation model ECHAM5—Part 1, *Tech. Rep. (349)*, 140 pp., Max Planck Inst. for Meteorol., Hamburg, Germany.
- Rummukainen, M. (2010), State-of-the-art with regional climate models, *WIREs Clim. Change*, *1*(1), 82–96.
- Sabin, T. P., R. Krishnan, J. Ghattas, S. Denvil, J.-L. Dufresne, F. Hourdin, and T. Pascal (2013), High resolution simulation of the South Asian monsoon using a variable resolution global climate model, *Clim. Dyn.*, *41*(1), 173–194, doi:10.1007/s00382-012-1658-8.
- Sass, B. H., et al. (2002), The operational DMI-HIRLAM system 2002-version, *Tech. Rep. (02-05)*, 60 pp., Danish Meteorol. Inst.
- Schulz, J.-P., L. Dümenil, and J. Polcher (2001), On the land surface-atmosphere coupling and its impact in a single-column atmospheric model, *J. Appl. Meteorol.*, *40*, 642–663.
- Sikka, D. R., and S. Gadgil (1980), On the maximum cloud zone and the ITCZ over Indian longitudes during the southwest monsoon, *Mon. Weather Rev.*, *108*, 1840–1853.
- Sinha, P., U. C. Mohanty, S. C. Kar, S. K. Dash, and S. Kumari (2013), Sensitivity of the GCM driven summer monsoon simulations to cumulus parameterization schemes in nested RegCM3, *Theor. Appl. Climatol.*, *112*(1), 285–306, doi:10.1007/s00704-012-0728-5.
- Sobel, A., and E. Maloney (2012), An Idealized semi-empirical framework for modeling the Madden-Julian oscillation, *J. Atmos. Sci.*, *69*, 1691–1705.
- Sommerfeld, A., O. Nikiema, A. Rinke, K. Dethloff, and R. Laprise (2015), Arctic budget study of intermember variability using HIRHAM5 ensemble simulations, *J. Geophys. Res. Atmos.*, *120*, 9390–9407, doi:10.1002/2015JD023153.
- Sperber, K. R., and H. Annamalai (2008), Coupled model simulations of boreal summer intraseasonal (30–50 day) variability, Part 1: Systematic errors and caution on use of metrics, *Clim. Dyn.*, *31*(2), 345–372, doi:10.1007/s00382-008-0367-9.
- Sperber, K. R., H. Annamalai, I. S. Kang, A. Kitoh, A. Moise, A. Turner, B. Wang, and T. Zhou (2013), The Asian summer monsoon: An intercomparison of CMIP5 vs. CMIP3 simulations of the late 20th century, *Clim. Dyn.*, *41*(9), 2711–2744, doi:10.1007/s00382-012-1607-6.
- Srinivas, C. V., D. Hariprasad, D. V. Bhaskar Rao, Y. Anjaneyulu, R. Baskaran, and B. Venkatraman (2012), Simulation of the Indian summer monsoon regional climate using advanced research WRF model, *Int. J. Climatol.*, *33*(5), 1195–1210, doi:10.1002/joc.3505.
- Su, H., and J. D. Neelin (2002), Teleconnection mechanisms for tropical Pacific descent anomalies during El Niño, *J. Atmos. Sci.*, *59*, 2694–2712.
- Tanré, D., J.-F. Geleyn, and J. M. Slingo (1984), First results of the introduction of an advanced aerosol-radiation interaction in the ECMWF low resolution global model, in *Aerosols and Their Climatic Effects*, edited by H. E. Gerber and A. Deepak, pp. 133–177, A. Deepak, Hampton, Va.
- Tiedtke, M. (1989), A comprehensive mass flux scheme for cumulus parameterization in large-scale models, *Mon. Weather Rev.*, *117*, 1917–1942.
- Tompkins, A. M. (2002), A prognostic parameterization for the subgrid-scale variability of water vapor and clouds in large-scale models and its use to diagnose cloud cover, *J. Atmos. Sci.*, *59*(12), 1779–1800.
- Trenberth, K. E., D. P. Stepaniak, and J. M. Caron (2002), Accuracy of atmospheric energy budgets from analyses, *J. Clim.*, *15*, 3343–3360.
- Undén, P., et al. (2002), HIRLAM-5 scientific documentation, *HIRLAM-5 Proj. Tech. Rep.*, 146 pp., Swedisch Meteorol. and Hydrol. Inst., Norrköpping, Sweden.
- Wang, B., and X. Xie (1997), A model for the boreal summer intraseasonal oscillation, *J. Atmos. Sci.*, *54*, 72–86.
- Watanabe, M., and F. F. Jin (2003), A moist linear baroclinic model: Coupled dynamical-convective response to El Niño, *J. Clim.*, *16*, 1121–1139.
- Wild, M., and E. Roeckner (2006), Radiative fluxes in the ECHAM5 general circulation model, *J. Clim.*, *19*, 3792–3809.
- Wild, M., B. Trüssel, A. Ohmura, C. Long, G. Köig-Langlo, E. G. Dutton, and A. Tsvetkov (2009), Global dimming and brightening: An update beyond 2000, *J. Geophys. Res.*, *114*, D00D13, doi:10.1029/2008JD011382.
- Yasunari, T. (1979), Cloudiness fluctuations associated with the northern hemisphere summer monsoon, *J. Meteorol. Soc. Jpn.*, *57*(3), 227–242.
- Yatagai, A., K. Kamiguchi, O. Arakawa, A. Hamada, N. Yasutomi, and A. Kitoh (2012), APHRODITE: Constructing a long-term daily gridded precipitation dataset for Asia based on a dense network of rain gauges, *Bull. Am. Meteorol. Soc.*, *93*, 1401–1415, doi:10.1175/BAMS-D-11-00122.1.
- Zhou, X., H. Matthes, A. Rinke, K. Klehmet, B. Heim, W. Dorn, D. Klaus, K. Dethloff, and B. Rockel (2014), Evaluation of Arctic Land snow cover characteristics, surface albedo, and temperature during the transition seasons from regional climate model simulations and satellite data, *Adv. Meteorol.*, *2014*, 604157, doi:10.1155/2014/604157.